PALEOCEANOGRAPHY, VOL. 14, NO. 5, PAGES 571-588, OCTOBER 1999

Variation of atmospheric CO_2 by ventilation of the ocean's deepest water

J. R. Toggweiler

Geophysical Fluid Dynamics Laboratory, National Oceanic and Atmospheric Administration
Princeton, New Jersey

Abstract. A new box model for glacial-interglacial changes in atmospheric CO_2 produces lower levels of atmospheric CO_2 without changes in biological production or nutrient chemistry. The model treats the boundary between middepth water and deep water as a chemical divide that separates low-CO_2 water above from high-CO_2 water below. Atmospheric CO_2 is reduced 21 ppm by reduced ventilation of the deep water below the divide. A further reduction of 36 ppm is due to $CaCO_3$ compensation in response to lower $CO_3^=$ below the divide. Colder surface temperatures account for an additional 23 ppm of CO_2 reduction. The new mechanism leaves the glacial atmosphere lighter in $\delta^{13}C$ than in preindustrial time, as seen in ice cores and fossil plant material. Bottom water below the divide becomes strongly depleted in $\delta^{13}C$ without a change in nutrient concentrations.

1. Introduction

Gas bubbles trapped in polar ice caps show that the CO_2 content of the Earth's atmosphere has changed systematically in the past along with the Pleistocene ice ages [*Jouzel et al.*, 1993]. The mechanism responsible for ice age CO_2 variations remains a mystery. *Broecker* [1982] demonstrated that the mechanism that controls atmospheric CO_2 on glacial/interglacial timescales must involve changes in the way that the ocean partitions carbon between the ocean and atmosphere; any change in atmospheric CO_2 initiated outside of the ocean is quickly damped by interaction with the ocean's huge CO_2 reservoir. Most of the mechanisms currently under discussion explain the lower levels of atmospheric CO_2 during glacial time in terms of a stronger biological pump [*Broecker*, 1982; *Sarmiento and Toggweiler*, 1984; *Siegenthaler and Wenk*, 1984; *Knox and McElroy*, 1984; *Dymond and Lyle*, 1985; *Broecker and Peng*, 1987; *Keir*, 1988; *Boyle*, 1988a; *Broecker and Peng*, 1989; *Martin*, 1990; *Lyle and Pisias*, 1990; *Keir*, 1990; *Marino et al.*, 1992; *Paillard et al.*, 1993; *Archer and Maier-Reimer*, 1994; *Broecker and Henderson*, 1998].

The strongest evidence in support of a stronger biological pump is the observation that the $\delta^{13}C$ difference between the surface ocean and deep ocean was 50% larger during glacial time [*Broecker*, 1982]. However, conventional biopump models increase the vertical $\delta^{13}C$ gradient the wrong way. Conventional models make the gradient larger by making the upper ocean and atmosphere heavier in $\delta^{13}C$. The observed gradient was 50% larger mainly because the deepest water in the ocean was lighter in $\delta^{13}C$ [*Curry et al.*, 1988; *Duplessy et al.*, 1988; *Kallel et al.*, 1988]. Atmospheric CO_2 trapped in ice cores was 0.3‰ lighter during glacial time [*Leuenberger et al.*, 1992]; fossil plant material suggests a 0.7‰ reduction [*Marino et al.*, 1992]. No conventional biopump model is able to reduce atmospheric CO_2 by 80 ppm and fit the glacial $\delta^{13}C$ observations at the same time.

Biopump models start from the proposition that the ocean's thermocline is a natural divide that separates the atmosphere and upper ocean from the deep ocean. Conventional biopump models lower atmospheric CO_2 by shifting CO_2 from the atmosphere and a thin layer of the upper ocean into a large volume of deep ocean. The upper ocean and atmosphere become isotopically heavy because the carbon pool above the thermocline is so small: a transfer of 1 mole of isotopically light carbon from a reservoir containing 100 moles of carbon to a reservoir with 1000 moles leaves the small sending reservoir considerably enriched in $\delta^{13}C$ while the big receiving reservoir becomes only slightly depleted.

The glacial $\delta^{13}C$ record is more easily understood if the ocean's chemical divide is deep in the ocean's interior. A deep divide makes the atmosphere, upper ocean, and the middle depths of the ocean the "big box" of the carbon system. A downward shift of isotopically light carbon in this case leaves the big upper box slightly enriched while the small volume of deep water below the divide is considerably depleted. Modest ancillary processes (e.g., cooler temperatures and reduced terrestrial biosphere) can easily convert a slightly enriched atmosphere into a depleted atmosphere. A deep divide is consistent with the results of *Sanyal et al.* [1995], who show that middepth water during glacial time had a higher pH and higher $CO_3^=$, properties expected for water that is part of a big upper box in contact with the atmosphere.

The idea of a deep chemical divide is not new. *Boyle* [1988a], *Keir* [1988], and *Sarmiento and Orr* [1991] put forward biological mechanisms that reduce atmospheric CO_2 by shifting isotopically light CO_2 from the upper half of the ocean into the lower half. Boyle called upon deeper remineralization of sinking organic matter. *Keir* [1988] and *Sarmiento and Orr* [1991] increased biological production in the Southern Ocean. However, the biological mechanisms discussed by *Boyle* [1988a], *Keir* [1988], and *Sarmiento and*

Paper number 1999PA900033.

Orr [1991] also shift PO_4 from the upper ocean into the deep ocean. The changes in PO_4 predicted by these models have not been observed, either in polar surface waters [*Boyle*, 1988b; *Keigwin and Boyle*, 1989] or in the deep ocean [*Boyle*, 1992].

It is suggested here that the chemical divide in the glacial ocean coincides with the water mass boundary separating deep waters formed in the Southern Ocean from the middepth and intermediate waters formed in the North Atlantic and elsewhere. A box model with seven ocean boxes shows how reduced ventilation of the deep water below such a boundary can lower atmospheric CO_2 and make it isotopically lighter at the same time. CO_2 in the model's deepest box becomes up to 1‰ lighter without changes in PO_4 and without changes in biological production or nutrient utilization. The new box model is built up as part of a sequence that starts with the three-box model of *Sarmiento and Toggweiler* [1984] and *Siegenthaler and Wenk* [1984]. The sequence includes models with three, four, six, and finally, seven boxes.

2. Biopump Model With a Generic High-Latitude Box

The three-box model of *Sarmiento and Toggweiler* [1984] and *Siegenthaler and Wenk* [1984], illustrated in Figure 1, is the simplest model to account for the partitioning of CO_2 between the ocean and atmosphere during preindustrial time. The ocean in this model consists of a low-latitude surface box (labeled l), a small high-latitude surface box (labeled h), and a large deep box (labeled d). The high-latitude box in this case is a generic high-latitude box with attributes of both the North Atlantic and the Southern Ocean. The surface boxes in the three-box model are very small: 97% of the ocean volume resides in the deep box.

Two circulation/exchange terms appear in the model. The term labeled T moves water up from the deep box into the low-latitude surface box, poleward into the h box, and then down again into the deep box. T represents the conveyor circulation that is initiated by deepwater formation in the North Atlantic. One expects the magnitude of T to be 15-20 Sv for the modern ocean [*Broecker*, 1991]. The term labeled f_{hd} is a bidirectional exchange or mixing term that ventilates the deep box directly through the high-latitude surface box. The formation of bottom water around Antarctica is one of the processes parameterized by f_{hd}.

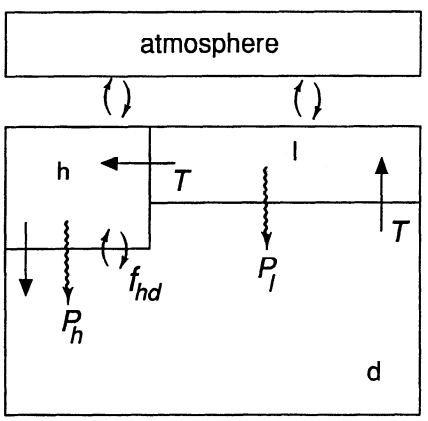

Figure 1. Schematic diagram of the three-box model of *Sarmiento and Toggweiler* [1984] and *Siegenthaler and Wenk* [1984].

The model assumes that the low-latitude biota convert all the PO_4 in the low-latitude box into sinking particles. This means that the PO_4 concentration in the low-latitude box is always zero and that the sinking flux P_l (in moles P yr^{-1}) is equal to TPO_{4d}. The nutrient uptake capacity of the high-latitude biota is assumed to be limited by factors other than nutrient supply (e.g., suboptimal light levels during winter). This leaves the high-latitude sinking flux P_h as a free parameter. PO_{4h} becomes a key diagnostic. Surface waters over a large area in the Southern Ocean have phosphate concentrations between 1.0 and 2.0 μmoles kg^{-1} [*Levitus et al.*, 1993]. Phosphate levels at the upper end of this range are close to the PO_4 level observed in the deep water around Antarctica (~2.2 μmoles kg^{-1}). This suggests that biological production in high-latitude surface waters is generally weak with respect to the PO_4 input from below.

The three-box model has one deep box but two ways to ventilate it. Herein lies the flexibility that allows the three-box model to describe the modern carbon system. This effect is illustrated in the deep-box oxygen balance in (1). The parameter $r_{O2:P}$ in (1) is the molar ratio linking O_2 uptake and PO_4 remineralization during the respiration of marine organic matter. O_{2h} is the oxygen concentration at saturation in the high-latitude box;

$$\frac{dO_{2d}}{dt} = (f_{hd} + T)(O_{2h} - O_{2d}) - r_{O2:P}(P_l + P_h) . \qquad (1)$$

Equation (1) simply says that sources of oxygen to the deep box due to the circulation terms f_{hd} and T are balanced at steady state by O_2 sinks due to P_l and P_h. However, P_l is also a function of T. Substituting TPO_{4d} for P_l and assuming steady state yields a simple expression for O_{2d} (equation (2)):

$$O_{2d} = O_{2h} - r_{O2:P}\frac{(TPO_{4d} + P_h)}{(f_{hd} + T)} . \qquad (2)$$

If P_h is small in relation to the other terms, (2) reduces to (3).

$$O_{2d} = O_{2h} - r_{O2:P}\, PO_{4d}\frac{T}{f_{hd} + T} \qquad (3)$$

For $T >> f_{hd}$ the term $T/(f_{hd} + T)$ on the right-hand side of (3) approaches unity. Plugging in 330 μmoles kg^{-1} for O_{2h}, 2.15 μmoles kg^{-1} for PO_{4d}, 170 for $r_{O2:P}$, and 0 for f_{hd}, one finds $O_{2d} = 330 - 360 = -30$ μmoles kg^{-1}. If the deep box is ventilated only by T, it remains in a state of perpetual anoxia no matter how much high-O_2 polar water is being added. Every mole of O_2 added by deepwater formation is consumed by the remineralization of sinking particles.

The high oxygen content of the real deep ocean requires a process like f_{hd} that adds high-oxygen polar water to the interior without creating additional sinking particles. In the con-

Table 1. Input Parameters for Three-Box Model

	Parameter Name	Value	Source
		Fixed Parameters	
Volume of the ocean	VT	1.292×10^{18} m^3	*Levitus* [1982]
Area of the ocean	AREA	349×10^{12} m^2	*Sverdrup et al.* [1942]
Mole volume of atmosphere	VATM	1.773×10^{20} moles	*Weast and Astle* [1979]
Depth of low-latitude box	ALZ	100 m	TS85
Depth of high-latitude box	AHZ	250 m	TS85
% area of high-latitude box	FH	15	TS85
Volume of low-latitude box	VL	2.97×10^{16} m^3	AREA(1–FH)ALZ
Volume of high-latitude box	VH	1.31×10^{16} m^3	(AREA)(FH)(AHZ)
Volume of deep box	VD	1.249×10^{18} m^3	VT–VL–VH
Temperature of low-latitude box	TEMPL	21.5°C	---
Temperature of high-latitude box	TEMPH	2.0°C	---
Salinity of the ocean	SAL	34.7	---
Corg/P in sinking particles	$r_{Corg:P}$	130	*Takahashi et al.* [1985]
% $CaCO_3$ in sinking particles	FCA	20	*Broecker and Peng* [1982]
Total C/P in sinking partricles	$r_{C:P}$	162.5	$r_{Corg:P}$ / (1–FCA)
Alk/P in sinking particles	$r_{Alk:P}$	50	2(FCA)$r_{C:P}$ – 15
O_2/P for remineralization of sinking particles	$r_{O2:P}$	169	*Takahashi et al.* [1985]
$\delta^{13}C$ of organic matter	$^{13}\varepsilon$	–23‰	TS85
Gas exchange piston velocity	PVL, PVH	3.0 m day^{-1}	TS85
Conveyor transport	T	20 Sv	---
		Variable Parameters	
Vertical exchange between high-latitude box and deep box	f_{hd}	3 - 300 Sv	
Sinking flux from high-latitude box	P_h	0.075 - 7.5 moles C m^{-2} yr^{-1}	

text of (3) the observed O_{2d}, ~170 μmoles kg^{-1}, requires that $T/(f_{hd} + T)$ must be ~0.4; that is, f_{hd} must exceed T. Similar considerations apply to atmospheric CO_2. The T-driven production of sinking particles transfers so much upper ocean CO_2 into the deep ocean that T acting alone would keep atmospheric CO_2 well below glacial levels. If f_{hd} exceeds T, on the other hand, much of the CO_2 remineralized from sinking particles is allowed to escape from the deep ocean back to the atmosphere.

The full carbon system requires a numerical model[1]. Each model in this paper is initialized with a first-guess partitioning of fixed pools of atmospheric and oceanic CO_2, $^{13}CO_2$, $^{14}CO_2$, oceanic PO_4, and oceanic alkalinity. The model is stepped forward, and model variables are shifted around between oceanic and atmospheric boxes until the variables reach steady state. *Toggweiler and Sarmiento* [1985, Table2] (hereafter TS85) give the total amounts of CO_2, PO_4, and alkalinity used to initialize the model. Equilibrium constants and a computer program by *Takahashi et al.* [1980] are used to determine the partial pressure of CO_2 in the surface boxes. TS85 (Table A1) gives air-sea fractionation factors for the carbon isotopes.

A full set of input parameters for the three-box model is given in Table 1. The Redfield ratio, $r_{Corg:P}$, linking the production and consumption of organic carbon to P_l and P_h is set to 130 after *Takahashi et al.* [1985]. Both sinking fluxes are assumed to contain 1 mole of $CaCO_3$ for every 4 moles of organic carbon. The ratio of total carbon to P in each sinking flux, $r_{C:P}$, is 162.5. There is no external input or sediment burial as all the organic matter and $CaCO_3$ sinking into the deep box is remineralized or dissolved.

The sensitivity of the full model is illustrated in Figure 2, where the output variables pCO_{2atm}, PO_{4h}, and O_{2d} are contoured over a parameter space defined by the forcing parameters f_{hd} and P_h. The vertical axis, $\log_{10}(f_{hd})$, spans a range

[1]FORTRAN source code for the three-box, four-box, six-box, and seven-box models in this paper is available on diskette or via Anonymous FTP from kosmos.agu.org, directory APEND (Username=anonymous, Password=guest). Diskette may be ordered from American Geophysical Union, 2000 Florida Avenue, N.W., Washington, DC 20009 or by phone at 800-966-2481; $15.00. Payment must accompany order.

present-day

glacial-like

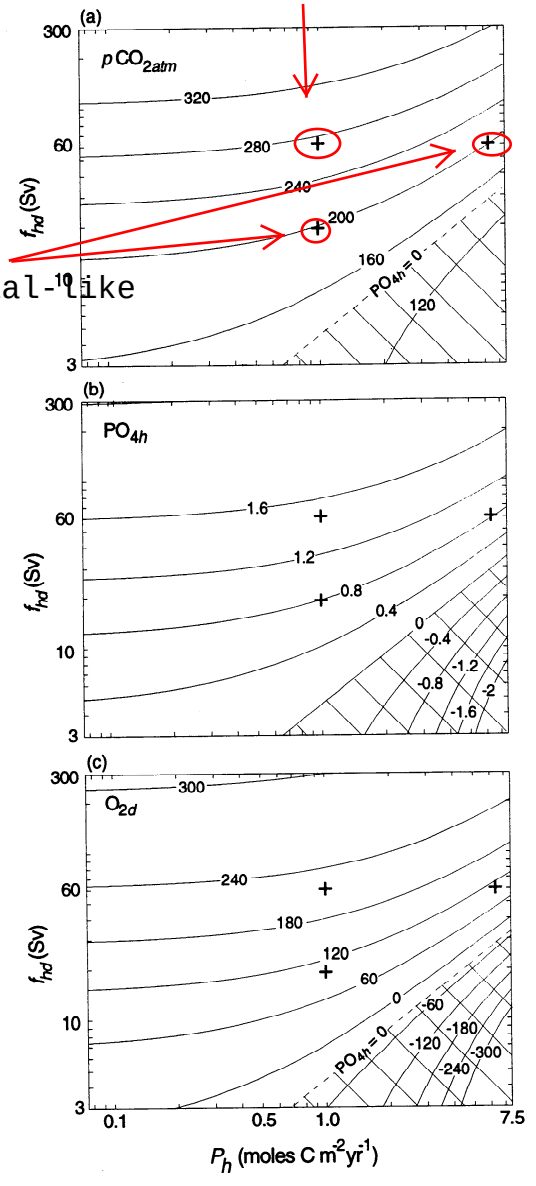

Figure 2. (a) Atmospheric CO_2 in ppm, (b) PO_{4h} in µmoles kg^{-1}, and (c) O_{2d} in µmoles kg^{-1} in the three-box model. The three variables are contoured over a parameter space defined by variations in f_{hd} and P_h. Input parameters are given in Table 1.

biological pump sinking rate

of 3-300 Sv, while the horizontal axis, $\log_{10}(P_h)$, spans 0.075-7.5 moles C m^{-2} yr^{-1}. T has been specified to be 20 Sv. The magnitude of P_h along the horizontal axis is given, for convenience, as a carbon flux per unit area, for example, $r_{C:P}P_h$ /AREA/FH.

Contours of atmospheric pCO_2 in Figure 2a and O_{2d} in Figure 2c are parallel to each other everywhere within the parameter space. This shows that the partitioning of CO_2 between the atmosphere and the deep box is controlled by the relative magnitudes of T, f_{hd}, and P_h much like the partitioning of oxygen in (2). There is relatively little sensitivity to P_h, except on the right-hand side, where P_h is very large. The relative magnitudes of T, f_{hd}, and P_h also control PO_{4h} in Figure 2b. T dilutes PO_{4h} by bringing PO_4-free low-latitude water into the h box. The f_{hd} increases PO_{4h} by adding PO_4-rich deep water from below. PO_{4h} becomes negative in the lower right-hand corner of the domain where P_h is large and f_{hd} is small.

A reasonable solution for the modern ocean is found just above the center of the parameter space with f_{hd} at ~60 Sv and P_h at ~1 mole C m^{-2} yr^{-1}. With these parameters the model atmosphere has a pCO_2 of ~275 ppm, and the high-latitude box has a PO_4 concentration of ~1.5 µmoles kg^{-1}. A glacial level of atmospheric CO_2 (~200 ppm) can be reached by reducing f_{hd} (moving down the plot) or by increasing P_h (moving to the right). In either case a glacial level of atmospheric CO_2 corresponds to a reduction in PO_{4h} from 1.50 to 0.80 µmoles kg^{-1}.

Figure 3 contrasts CO_2, PO_4, and $\delta^{13}C$ levels in a high-CO_2 state and two low-CO_2 states of the three-box model. Figure 3a gives total CO_2 concentrations (TCO_2) within the boxes and the CO_2 partial pressures for the atmospheric and surface ocean boxes above. Figure 3b gives oceanic PO_4. Figure 3c gives the $\delta^{13}C$ for the ocean boxes and for the atmosphere. Results from the high-CO_2 state (f_{hd} = 60 Sv and P_h = 1.0 moles C m^{-2} yr^{-1}) are on the left. Atmospheric pCO_2 in the high-CO_2 state is 272 ppm; PO_{4h} is 1.48 µmoles kg^{-1}.

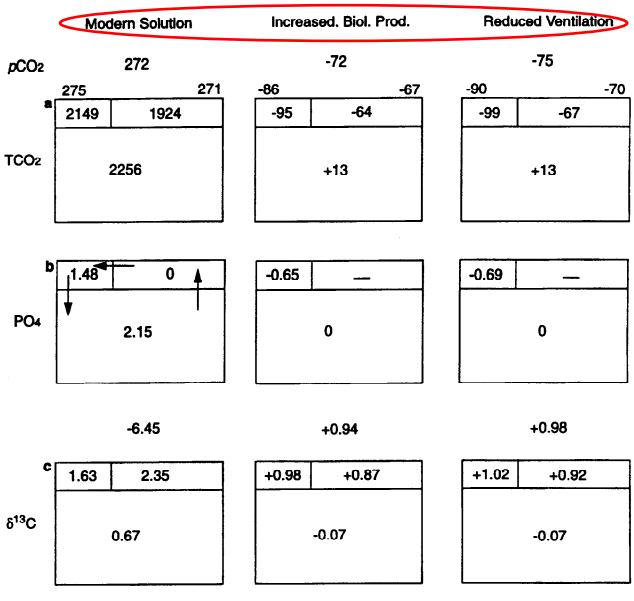

Figure 3. Solutions of the three-box model for (a) pCO_2 and total CO_2 concentrations (TCO_2), (b) PO_4, and (c) $\delta^{13}C$ for a high-CO_2 modern state (in the left column, f_{hd} = 60 Sv and P_h = 1.0 moles C m^{-2} yr^{-1}) and two low-CO_2 states (middle and right columns). The low-CO_2 state in the middle is produced by increasing P_h to 6.3 moles C m^{-2} yr^{-1} with f_{hd} constant. The low-CO_2 state on the right is produced by reducing f_{hd} to 19 Sv with P_h constant. Results for the two low-CO_2 states are given as differences from the high-CO_2 state. The increase in P_h and reduction in f_{hd} are the only changes being made to reduce atmospheric CO_2, no changes have been made to reflect colder glacial temperatures, a higher salinity, or a smaller terrestrial biosphere. The alkalinity difference between the d box and the l box is nearly the same in all three solutions, 107.5 µeq kg^{-1}.

The low-CO_2 state in the middle column of Figure 3 is produced by increasing biological production in the high-latitude box from 1.0 up to 6.3 moles C m^{-2} yr^{-1}. The low-CO_2 state in the column on the right is produced by reducing f_{hd} from 60 to 19 Sv. Results for the two low-CO_2 states are given as differences from the high-CO_2 state. PO_{4h} decreases by 0.65 and 0.69 μmoles kg^{-1}. Atmospheric CO_2 is drawn down by 72 and 75 ppm to glacial levels of ~200 ppm. TCO_2 differences between the low-latitude surface box and the deep box are partitioned in both cases between a large TCO_2 decrease above (~ −65 μmoles kg^{-1}) and a small TCO_2 increase below (+13 μmole kg^{-1}).

Increased polar production and reduced ventilation increase the $\delta^{13}C$ of the atmosphere and upper ocean by 0.9-1.0‰ (Figure 3c). The $\delta^{13}C$ of the big deep box is barely perturbed, however, becoming only 0.07‰ lighter in both low-CO_2 states. These results run counter to glacial observations. *Broecker* [1982] proposed that a large reduction in the size of the terrestrial biosphere during glacial time [*Shackleton*, 1977] might have negated the positive $\delta^{13}C$ shift predicted for the upper ocean while it produced a negative $\delta^{13}C$ shift in the deep ocean. The terrestrial biosphere effect is now seen as being only −0.35‰ [*Curry et al.*, 1988; *Duplessy et al.*, 1988]. This is too small to mask a 0.9-1.0‰ $\delta^{13}C$ increase in the upper ocean.

The three-box mechanism was seen as a significant breakthrough in its day because it showed that nutrient utilization over a relatively small part of the ocean's surface could govern the pCO_2 of the atmosphere and the rest of the surface ocean. However, *Boyle* [1988b] and *Keigwin and Boyle* [1989] soon showed that PO_4 levels in Antarctic waters south of the polar front were fairly constant over the past 50 kyrs and did not vary with atmospheric CO_2. Indeed, a summary article by *Boyle* [1992] seems to indicate that atmospheric CO_2 was lowered by 80 ppm without significant changes in the distribution of PO_4 anywhere.

In sections 3 and 4 the three-box model is transformed into a model with seven boxes. One feature of the three-box model is retained while three features are altered. The first feature to be altered is the generic high-latitude box. The old high-latitude box is split into two so that the sinking branch of the T circulation is directed into a separate North Atlantic box. This leaves the original high-latitude box as a Southern Ocean box. The upwelling branch of the T circulation is then moved from the low-latitude box into the southern box so that the southern box becomes a region of net upwelling rather than net sinking. These modifications convert the three-box model into the four-box model in the next section. The third feature to be altered is the deep box itself. The deep box is divided into two parts, a part ventilated from the North Atlantic box via T and a part ventilated from the southern box via f_{hd}. This modification is carried out in two steps leading to the six- and seven-box models in section 4. The three new models in this paper retain the idea that the ventilation of the deep ocean can be described by processes that operate like T and f_{hd} in the three-box model.

3. The Southern Ocean As a Region of Upwelling

Oceanographers have known for a long time that deep water upwells to the surface in the Southern Ocean because of Ekman pumping [*Deacon*, 1937; *Sverdrup et al.*, 1942, *Wyrtki*, 1961]. More deep water upwells to the surface than is returned to the deep ocean as new bottom water. *Toggweiler and Samuels* [1993, 1995] have suggested that the upwelling branch of *Broecker*'s [1991] conveyor occurs entirely in the Southern Ocean as part of Ekman divergence south of the Antarctic Circumpolar Current (ACC). The significance of shifting the upwelling branch of the conveyor into the Southern Ocean can be demonstrated in a rudimentary way by simply reversing the direction of T in the three-box model.

Equation (4) gives the CO_2 balance for the deep box of the three-box model in Figure 1:

$$\frac{dTCO_{2d}}{dt} = (f_{hd} + T)(TCO_{2h} - TCO_{2d}) + r_{C:P}(P_l + P_h). \quad (4)$$

Input of low-CO_2 water from the h box by f_{hd} and T is balanced by the remineralization of CO_2 from the particle fluxes P_l and P_h. Substituting TPO_{4d} for P_l at steady state yields

$$TCO_{2d} - TCO_{2h} = r_{C:P}\left(\frac{TPO_{4d}}{f_{hd} + T} + \frac{P_h}{f_{hd} + T}\right). \quad (5)$$

Equation (6) is the balance equation for PO_4 in the high-latitude box:

$$\frac{dPO_{4h}}{dt} = T(PO_{4l} - PO_{4h}) + f_{hd}(PO_{4d} - PO_{4h}) - P_h. \quad (6)$$

With $PO_{4l} = 0$ at steady state, (6) becomes

$$PO_{4h} = PO_{4d}\frac{f_{hd}}{(f_{hd} + T)} - \frac{P_h}{(f_{hd} + T)}. \quad (7)$$

The CO_2 system in (5) can be simplified by eliminating $CaCO_3$ from P_l and P_h. This eliminates TCO_2 differences between the boxes due to alkalinity differences. The CO_2 system can be simplified further by eliminating temperature differences between the boxes. The carbon system in (5) is now a simple organic carbon pump. If P_h is also assumed to be small in relation to other terms and gas exchange rates are assumed to be high, then TCO_{2h} approaches TCO_{2l}, and (5) can be rewritten as

$$TCO_{2d} - TCO_{2l} \sim r_{Corg:P}\, PO_{4d}\frac{T}{f_{hd} + T}. \quad (8)$$

At the limit of small P_h, (4) becomes

$$PO_{4h} = PO_{4d}\frac{f_{hd}}{f_{hd} + T}. \quad (9)$$

$TCO_{2d} - TCO_{2l}$ in (8) is the amount of CO_2 trapped in the deep box by the organic pump. $TCO_{2d} - TCO_{2l}$ is large when atmospheric CO_2 is low. Like O_{2d} in (3), $TCO_{2d} - TCO_{2l}$ in (8) is a simple function of PO_{4d} and the relative magnitudes

of T and f_{hd}. PO_{4h} in (9) is also a simple function of PO_{4d} and the relative magnitudes of T and f_{hd}.

If the T circulation is reversed so that the upwelling branch of T is in the h box and the sinking branch is in the l box, the CO_2 balance in the deep box becomes

$$\frac{dTCO_{2d}}{dt} = T(TCO_{2l} - TCO_{2d}) + f_{hd}(TCO_{2h} - TCO_{2d}) \quad (10)$$
$$+ r_{C:P}\,(P_l + P_h)\,.$$

Substituting TPO_{4_h} for P_l at steady state yields

$$TCO_{2d}(f_{hd} + T) - TCO_{2l}T - TCO_{2h}f_{hd} \quad (11)$$
$$= r_{C:P}\ PO_{4h}T + r_{C:P}\,P_h\ .$$

The complementary balance expression for PO_{4h} is

$$PO_{4h} = PO_{4d} - \frac{P_h}{f_{hd} + T}\ . \quad (12)$$

Note that the factor $f_{hd}/(f_{hd} + T)$ that is multiplied by PO_{4d} in (7) and (9) is gone in (12). This is because the T circulation no longer dilutes PO_{4h} with low-latitude water.

Using the same assumptions as above, i.e., no $CaCO_3$, no temperature differences, weak P_h, and fast gas exchange, (11) and (12) become

$$TCO_{2d} - TCO_{2l} \sim r_{Corg:P}\ PO_{4d}\ \frac{T}{f_{hd} + T} \quad (13)$$

and

$$PO_{4h} = PO_{4d}\,. \quad (14)$$

Equation (13) is identical to (8). This says that the amount of CO_2 trapped in the deep box is more or less the same whether deep water upwells into the h box or the l box. PO_{4h}, on the other hand, is identical to PO_{4d}. With upwelling in the h box and weak biological production, PO_{4h} is compelled to stay close to PO_{4d}. The key to this result is that T and f_{hd} still carry out their same roles with regard to O_{2d} and atmospheric CO_2: T still cycles PO_4 up from the deep box and generates sinking particles, and f_{hd} continues to add oxygen to the deep box and to allow remineralized CO_2 to escape to the atmosphere.

The decoupling of atmospheric CO_2 from PO_{4h} implied by (13) and (14) can be demonstrated explicitly in the four-box model in Figure 4. The four-box model has a separate surface box, labeled n, to represent the sinking region of the North Atlantic. The h box of the three-box model is now a Southern Ocean box. The conveyor circulation is routed up through the h box, through the low-latitude box, and into the North Atlantic box. The PO_4 content of the n box is always zero because all the water coming into the n box comes from the nutrient-depleted l box. There is no flux of sinking particles from the n box in the four-box model. The area of the h box is kept at 15%, while 10% of the area of the l box is given over to the n box. Table 2 gives additional input parameters for the four-box model.

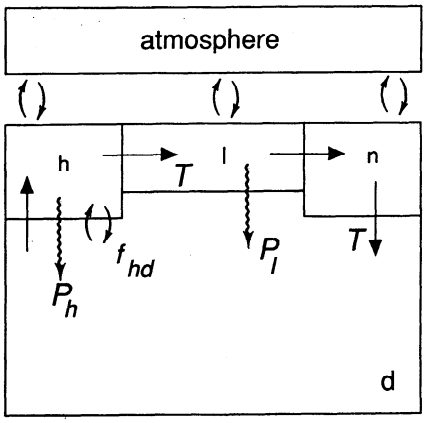

Figure 4. Schematic diagram of the four-box model.

The sensitivity of atmospheric CO_2, PO_{4h}, and O_{2d} to variations in f_{hd} and P_h in the four-box model is illustrated in Figure 5. T is again specified to be 20 Sv. The response of atmospheric CO_2 and O_{2d} to reduced f_{hd} is similar to the response in the three-box model (Figure 2). The response of PO_{4h} is much different. Atmospheric CO_2 is easily reduced to glacial levels in the center of the parameter space with minimal changes in PO_{4h}. P_h must exceed 3 moles C m^{-2} yr^{-1} before biological production in the h box brings about a strong covariance between atmospheric CO_2 and PO_{4h}.

Figure 6 contrasts the PO_4 and CO_2 concentrations in high- and low-CO_2 states of the four-box model. As in Figure 3, f_{hd} is set at 60 Sv, and P_h is set at 1.0 moles C m^{-2} yr^{-1} for the high-CO_2 state on the left. The atmospheric pCO_2 in this case is 264 ppm; switching the T term from sinking to upwelling in the h box does not change atmospheric CO_2 very much. The big difference between the three- and four-box models is the fact that the four-box model has strong regional differences in pCO_2. The difference in pCO_2 between the h box and the atmosphere is 297 – 264 = 33 ppm compared with 275 – 272 = 3 ppm in the three-box model. The ΔpCO_2 between the n box and the atmosphere is 226 – 264 = –38 ppm. Much of the CO_2 remineralized in the deep box cycles back up to the surface by outgassing through the h box. Much of the CO_2 taken up by the low-latitude biota comes directly from the atmosphere.

For the low-CO_2 state in the middle column of Figure 6, P_h is held constant while f_{hd} is reduced from 60 to 15 Sv. Differences from the high-CO_2 state are given in the right-hand column. The reduction of atmospheric CO_2 by 64 ppm is accompanied by a very modest change in PO_{4h}, –0.16 μmoles kg^{-1}. The h box continues to be a strong source of CO_2 to the atmosphere, albeit a smaller source than before. Reduced mixing between the h box and the deep box allows less CO_2 to pass through the h box to the atmosphere in relation to the CO_2 demand generated by T in the low-latitude box. A lower gas exchange rate in the h box would be able to reduce atmospheric CO_2 in much the same way.

The Pandora model of *Broecker and Peng* [1987] and the Cyclops model of *Keir* [1988] have circulation schemes that

Table 2. Additional Input Parameters for Four-Box Model

	Parameter Name	Value	Source
		Fixed Parameters	
Depth of northern box	ANZ	250 m	---
Depth of southern box	AHZ	250 m	---
% area of northern box	FN	15	---
% area of southern box	FH	10	---
Volume of low-latitude box	VL	2.62×10^{16} m^3	AREA(1–FN–FH)ALZ
Volume of northern box	VN	0.87×10^{16} m^3	(AREA)(FN)(ANZ)
Volume of southern box	VH	1.31×10^{16} m^3	(AREA)(FH)(AHZ)
Volume of deep box	VD	1.244×10^{18} m^3	VT–VL–VN–VH
Temperature of northern box	TEMPN	3.0°C	---
Temperature of southern box	TEMPH	1.0°C	---
		Variable Parameters	
Vertical exchange between high-latitude box and deep box	f_{hd}	3 - 300 Sv	
Sinking flux from high-latitude box	P_h	0.075 - 7.5 moles C m^{-2} yr^{-1}	

feature upwelling in the Southern Ocean, but neither model reveals the kind of decoupling between atmospheric CO_2 and Southern Ocean nutrients seen here. This is because Pandora and Cyclops both have 3-4 times more biological production per unit upwelling in their Antarctic surface boxes, i.e., much higher P_h. The standard solutions for these models lie in a region of parameter space far to the right in Figure 5 where P_h is important. A high level of biological production in Antarctic waters is justified in the Pandora and Cyclops models by the need to draw Antarctic PO_4 down to a level where it matches the observed surface PO_4 across the entire Southern Ocean. However, most of the observed PO_4 drawdown in the Southern Ocean occurs in subantarctic waters that are physically separated from the area where deep upwelling and deep ventilation takes place.

4. Deep Ocean With Internal Boundaries

In this section, two internal boundaries are introduced to divide the deep box of the four-box model into three regimes. The first boundary isolates thermocline and intermediate-depth water from the rest of the deep box. Thermocline and intermediate waters are ventilated by T and direct exchange with the low-latitude surface box. The second internal boundary separates the rest of the deep box into a middepth box ventilated from the north by T and a deep box ventilated from the south by f_{hd}.

4.1. Six-Box Ocean

Figure 7 shows a six-box model with one internal boundary. Thermocline and intermediate waters below the low-latitude box are identified as box m. The m box is assumed to be 900 m thick. The h box in the four-box model has been renamed p; a second new box labeled s is added to differentiate "subantarctic" surface waters from "polar" surface waters. Deep water upwelling into the polar box as part of the T circulation passes through the subantarctic box and downwells into the m box. Water from the m box upwells again into the n box before sinking again into the deep box. A new mixing term f_{lm} exchanges water between the m box and the low-latitude surface box. The upwelling of deep water associated with T is confined to the polar box along with the surface to deep mixing parameterized by f_{hd}. The parameter f_{hd} is renamed f_{pd} to maintain consistency with the new box names. The area of the p box is limited to 5% of the ocean's surface area. The subantarctic and northern boxes are each assumed to occupy 10%.

P_p, P_s, and P_n represent the sinking fluxes from the p, s, and n boxes. PO_{4n} is nonzero because the n box receives water from the m box instead of the l box. In the presentation below, P_n and P_p will be assigned specific values while P_s is allowed to vary across a parameter range like P_h in the three- and four-box models. A new term γ_m represents the fraction of the sinking fluxes from the l and s boxes that is remineralized in the m box. The remainder, $1-\gamma_m$, is remineralized in the deep box. Table 3 lists parameter values for the six-box model.

The sensitivity of atmospheric CO_2 and subantarctic PO_4 to variations in f_{pd} and P_s is illustrated in Figure 8. f_{pd} varies from 3 to 300 Sv as before, while P_s varies from 0.15 to 15 moles C m^{-2} yr^{-1}. T is fixed at 20 Sv, P_p is fixed at 1.0 moles C m^{-2} yr^{-1}, and P_n is fixed at 3 moles C m^{-2} yr^{-1}. Contours of atmospheric CO_2 in Figure 8a are spread farther apart than in Figure 5. A glacial level of atmospheric CO_2 is reached only in the lower right-hand corner of the parameter space.

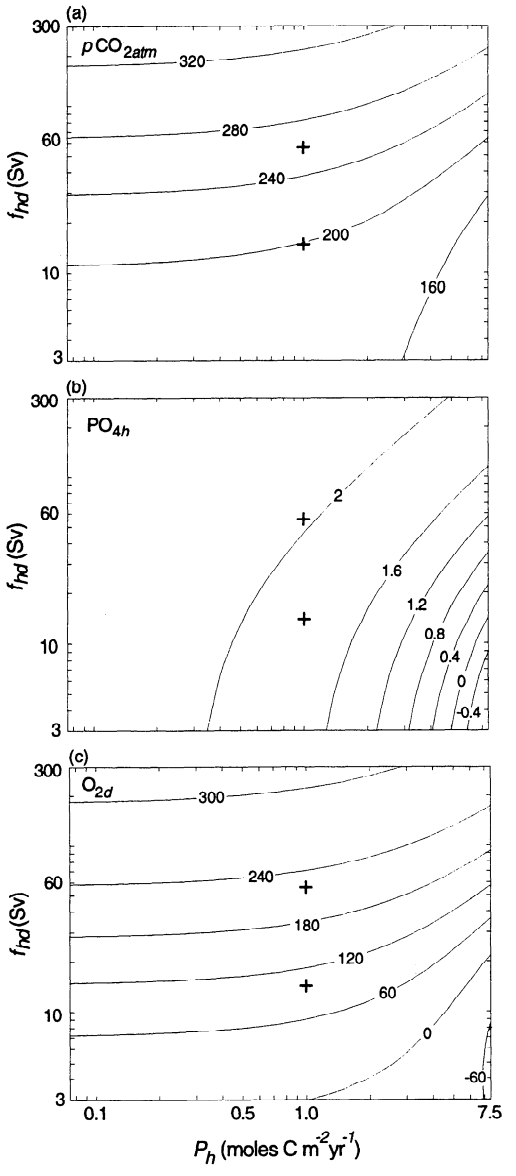

Figure 5. (a) Atmospheric CO_2, (b) PO_{4h}, and (c) O_{2d} in the four-box model. Variables are contoured over a parameter space defined by variations in f_{hd} and P_h. Input parameters are given in Tables 1 and 2.

Contours of PO_{4s} are nearly vertical in Figure 8b. Decreasing PO_{4s} from 2.1 μmoles kg^{-1} on the left-hand side all the way to zero on the right reduces atmospheric CO_2 by ~30 ppm. A characteristic subantarctic PO_4 level of ~1.25 μmoles kg^{-1} is achieved with P_s at 3 moles C m^{-2} yr^{-1}. The average PO_4 concentration in the polar and subantarctic boxes, taking into account the relative areas of the two boxes, is 1.63 μmoles kg^{-1}. This value is similar to the PO_4 concentrations in the single Antarctic surface boxes in Pandora and Cyclops.

Figure 9 contrasts PO_4, $\delta^{13}C$, TCO_2, and pCO_2 levels in high- and low-CO_2 states of the six-box model. The high-CO_2 state in the column on the left (f_{pd} = 60 Sv) has an atmospheric pCO_2 of 287 ppm. The low-CO_2 state in the middle column (f_{pd} = 12 Sv) has a pCO_2 of 233 ppm. As before, the column on the right gives differences between the high- and low-CO_2 states. A reduction of f_{pd} from 60 to 12 Sv reduces atmospheric CO_2 by 54 ppm. With 20 Sv of deep water upwelling in a smaller box the PO_4 concentration in the polar box is almost unchanged between the two states. Indeed, no PO_4 change in the six-box model is larger than 0.05 μmoles kg^{-1}.

The new m box receives a direct input of water from the subantarctic box which is nearly in equilibrium with atmospheric CO_2. TCO_2 concentrations in the m box, l box, s box, and n box all go down by 40-50 μmoles kg^{-1}. The CO_2 removed from m box, the atmosphere, and the other surface boxes shows up as a 24 μmoles kg^{-1} increase in the TCO_2 of the deep box. The increase in $TCO2_d$ in the six-box model is twice the increase seen in the three- and four-box models. The TCO_2 of the polar box knows about the high TCO_2 concentrations in the deep box and does not drop nearly as much as the TCO_2 in the other surface boxes. This means that the pCO_2 of the polar box stays relatively high and the reduction in atmospheric CO_2 per unit reduction in f_{pd} is not as great as in the three- or four-box models.

Addition of the m box has a significant effect on the partitioning of $\delta^{13}C$ changes between the upper ocean and deep ocean. The increase in $\delta^{13}C$ in the atmosphere and s, l, and n boxes is only 0.4-0.7‰ compared with 0.9-1.1‰ in the three- and four-box models. The $\delta^{13}C$ decrease in the deep box is 3 times larger than before at −0.20‰.

4.2. $CaCO_3$ Compensation and $CO_3^=$ in the Deep Box

Higher concentrations of CO_2 in seawater reduce the concentration of carbonate ion $CO_3^=$. Lower $CO_3^=$ in the deep ocean is more corrosive toward $CaCO_3$ sediments. Persistent-

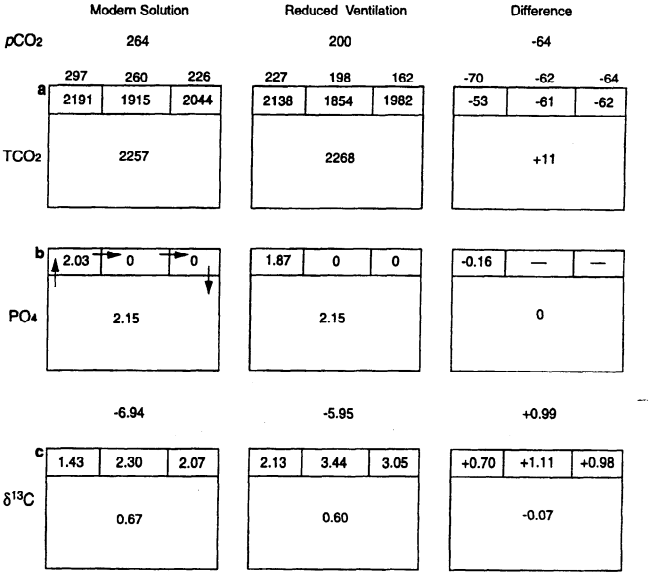

Figure 6. Solutions of the four-box model for (a) CO_2, (b) PO_4, and (c) $\delta^{13}C$ in a high-CO_2 state (in the left column, f_{hd} = 60 Sv and P_h = 1.0 moles C m^{-2} yr^{-1}) and a low-CO_2 state (middle column). The low-CO_2 state is produced by reducing f_{hd} from 60 to 15 Sv with P_h constant. The right column gives differences between the high- and low-CO_2 states. The alkalinity difference between the d box and the l box is 108 μeq kg^{-1} in both states.

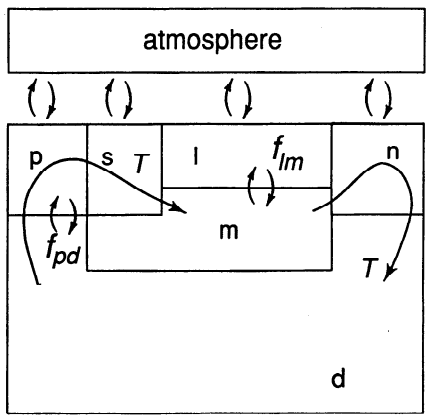

Figure 7. Schematic diagram of the six-box model. Wavy arrows denoting particle fluxes from the four surface boxes have been omitted for clarity.

ly lower $CO_3^=$ reduces the area of seafloor where $CaCO_3$ accumulates and disrupts the balance between the global burial rate of $CaCO_3$ and the input of Ca^{++} and CO_2 by rivers. If Ca^{++} input exceeds Ca^{++} removal for an extended period of time, the ocean becomes more alkaline, and the pCO_2 in the atmosphere and surface ocean drops. The decline in atmospheric CO_2 stops only when the $CO_3^=$ content of the deep ocean rises to a level that restores the original $CaCO_3$ burial rate. This effect is identified by *Broecker and Peng* [1987] as $CaCO_3$ compensation.

One expects the 24 μmole kg^{-1} increase in the TCO_2 of the deep box in Figure 9a to trigger a significant $CaCO_3$ compensation response. Figure 10 shows contours of the $CO_3^=$ content of the deep box over the same f_{pd} versus P_s parameter space as in Figure 8. The symbols L and H give the positions of the low- and high-CO_2 states in Figure 9. The deep box $CO_3^=$ at position H is 86 μmoles kg^{-1}. Reducing f_{pd} from 60 to 12 Sv decreases $CO_3^=$ to 74 μmoles kg^{-1}, a drop of 12 units. A comparable $CO_3^=$ response in the three- or four-box models would be ~6 μmoles kg^{-1}.

$CaCO_3$ compensation can be simulated by allowing the total amount of ocean alkalinity and TCO_2 to increase in a 2:1 ratio as if $CaCO_3$ weathering is exceeding $CaCO_3$ burial. Here the initial alkalinity and TCO_2 in each of the six ocean boxes is systematically increased until the final $CO_3^=_d$ at position L rises to 83 μmoles kg^{-1}, 3 μmoles kg^{-1} below the high-CO_2 state at position H. This leaves the deep ocean slightly more corrosive than before, as observed in glacial sediments of the deep Atlantic and Indian Oceans [*Catubig et*

Table 3. Input Parameters for Six-Box Model

	Parameter Name	Value	Source
		Fixed Parameters	
Depth of subantarctic box	ASZ	250 m	---
Depth of south polar box	APZ	250 m	---
Depth of thermocline box	AMZ	900 m	---
% area of northern box	FN	10	---
% area of subantarctic box	FS	10	---
% area of south polar box	FP	5	---
Volume of low-latitude box	VL	2.62×10^{16} m^3	AREA(1–FN–FS–FP)ALZ
Volume of northern box	VN	0.87×10^{16} m^3	(AREA)(FN)(ANZ)
Volume of subantarctic box	VS	0.87×10^{16} m^3	(AREA)(FS)(ASZ)
Volume of south polar box	VP	0.44×10^{16} m^3	(AREA)(FP)(APZ)
Volume of thermocline box	VM	0.297×10^{18} m^3	AREA(1–FN–FP)AMZ
Volume of deep box	VD	0.947×10^{18} m^3	VT–VL–VN–VS–VP–VM
Temperature of subantarctic box	TEMPS	8.0°C	---
Temperature of south polar box	TEMPP	1.0°C	---
Conveyor transport	T	20 Sv	
Mixing between l and m boxes	f_{lm}	40 Sv	---
Sinking flux from n box	P_n	3.0 moles C m^{-2} yr^{-1}	---
Sinking flux from p box	P_p	1.0 moles C m^{-2} yr^{-1}	
Fraction P_l, P_s remineralized in m box	γ_m	0.80	---
Fraction P_l, P_s remineralized in d box	---	0.20	$(1-\gamma_m)$
		Variable Parameters	
Vertical Exchange between polar box and deep box	f_{pd}	3 - 300 Sv	
Sinking flux from subantarctic box	P_s	0.15 - 15.0 moles C m^{-2} yr^{-1}	

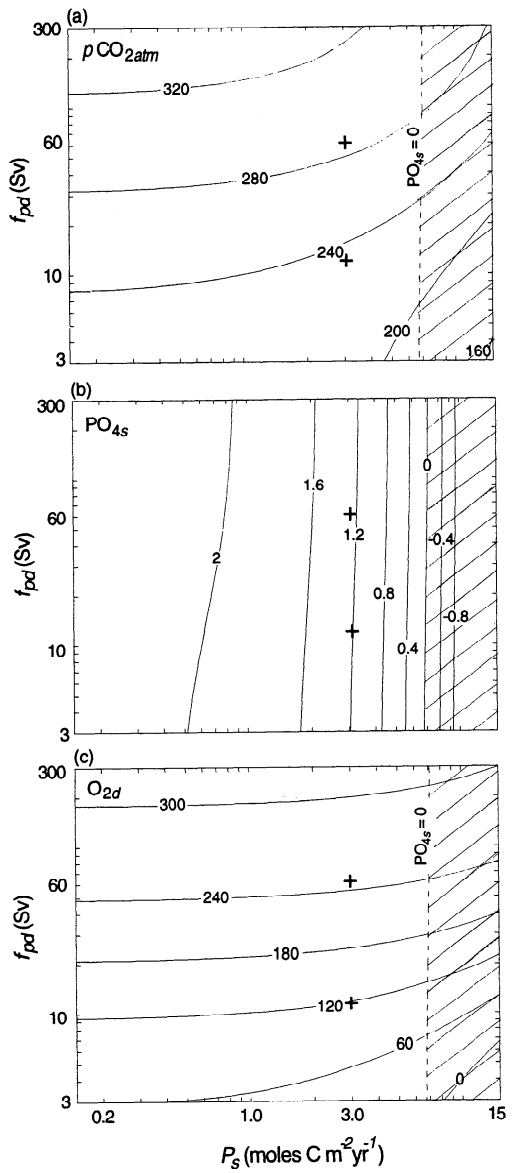

Figure 8. (a) Atmospheric CO_2, (b) subantarctic PO_{4s}, and (c) O_{2d} in the six-box model. Variables are contoured over a parameter space defined by variations in f_{pd} and P_s. P_p has been set to 1.0 moles C m^{-2} yr^{-1}, and P_n has been set to 3.0 moles C m^{-2} yr^{-1}. Other input parameters are given in Table 3.

al., 1998]. A 9 μmole kg^{-1} increase in $CO_3{}^{=}{}_d$ requires 30 μeq kg^{-1} more alkalinity and 15 μmoles kg^{-1} more TCO_2 in the initial state. The pCO_2 of the atmosphere is thereby reduced by an additional 10 ppm. The 54 ppm decrease in Figure 9 becomes a 64 ppm reduction after $CaCO_3$ compensation.

4.3. Seven-Box Ocean

A new interior box is inserted between the m and d boxes of the six-box model to make the seven-box model in Figure 11. The new box, labeled a for "Atlantic" layer, receives the sinking water from the northern surface box. The T circulation entering the a box from the n box passes into the deep box and upwells to the surface again in the p box. The new a box, like the m box, is an upper ocean box whose CO_2 content follows the CO_2 content of the l box and the atmosphere. The a box is initially 2000 m thick, i.e., half the volume of the entire ocean. This clearly makes the atmosphere and the l, m, and a boxes together the big box of the carbon system. Despite the similarities between the a box and North Atlantic Deep Water (NADW) the intent here is to have the a box represent all the ocean's middepth water between 1000 and 3000 m.

Two γ terms appear in the seven-box model. The first, γ_m, specifies the fraction of P_l and P_s remineralized in the m box as in the six-box model. The remainder, $1-\gamma_m$, is split equally between the a and d boxes. The second, γ_a, specifies the fraction of P_n remineralized in the a box. Table 4 lists new parameter values for the seven-box model.

The sensitivity of atmospheric CO_2 and the $CO_3{}^{=}$ and O_2 contents of the deep box to variations in f_{pd} and P_s is illustrated in Figure 12. Contours of atmospheric CO_2 in Figure 12a are spread much farther apart than in Figure 8. Contours of $CO_3{}^{=}$ in Figure 12b are squeezed much closer together. As the thickness of the a box is increased, the remineralized CO_2 trapped in the deep box is concentrated in a smaller and smaller volume. Higher CO_2 in the deep box makes it more difficult to reduce atmospheric CO_2 directly via f_{pd}, hence the greater spread between contours. However, higher CO_2 concentrations in the deep box produce much lower levels of $CO_3{}^{=}$. The $CO_3{}^{=}$ concentration in the deep box drops from 88 μmoles kg^{-1} with f_{pd} at 60 Sv (position H) to 59 μmoles kg^{-1} with f_{pd} at 10 Sv (position L), a decrease of 29 μmoles kg^{-1}.

Figure 13 contrasts PO_4 and CO_2 concentrations for two solutions of the seven-box model. The column on the left shows a high-CO_2 state at 271 ppm (f_{pd} = 60 Sv). The middle column shows a low-CO_2 state at 250 ppm (f_{pd} = 10 Sv). The column on the right gives differences between the high- and low-CO_2 states. TCO_2 levels in the l, m, and a boxes are reduced by 18, 19, and 16 μmoles kg^{-1}, respectively, in accord with a 22 ppm reduction in atmospheric CO_2. The TCO_2 in the deep box, meanwhile, increases by 64 μmoles kg^{-1}! Changes in TCO_2 in Figure 13 completely reverse the pattern seen in the three- and four-box models: TCO_2 changes are now largest in the deep box because it is the small box of the system. With such a large increase in TCO_{2d}, atmospheric CO_2 drops by only 21 ppm. As in the six-box model, changes in PO_4 between the high- and low-CO_2 states are very small, no more than 0.05 μmoles kg^{-1} in any box. Reducing f_{pd} from 60 to 10 Sv lowers the oxygen content of the deep box by 156 μmoles kg^{-1}. This is a large reduction, but the deep box remains fairly well oxygenated (Figure 12c).

The target for $CaCO_3$ compensation in the seven-box model is an increase in $CO_3{}^{=}{}_d$ at position L up to 85 μmoles kg^{-1}, a 26 μmole kg^{-1} increase. This requires 120 μeq kg^{-1} of additional alkalinity and 60 μmoles kg^{-1} of additional TCO_2. The extra alkalinity drives atmospheric CO_2 from 250 ppm down to 212 ppm for a total drop of 59 units. The pH of the a box rises by 0.17 units from its initial state, while it drops slightly in the deep box. Sixty-four percent of the total drop in pCO_2 is due to $CaCO_3$ compensation in response to low $CO_3{}^{=}$ in the deep box.

Biopump models by *Boyle* [1988a] and *Archer and Maier-Reimer* [1994] also reduce atmospheric CO_2 through a large

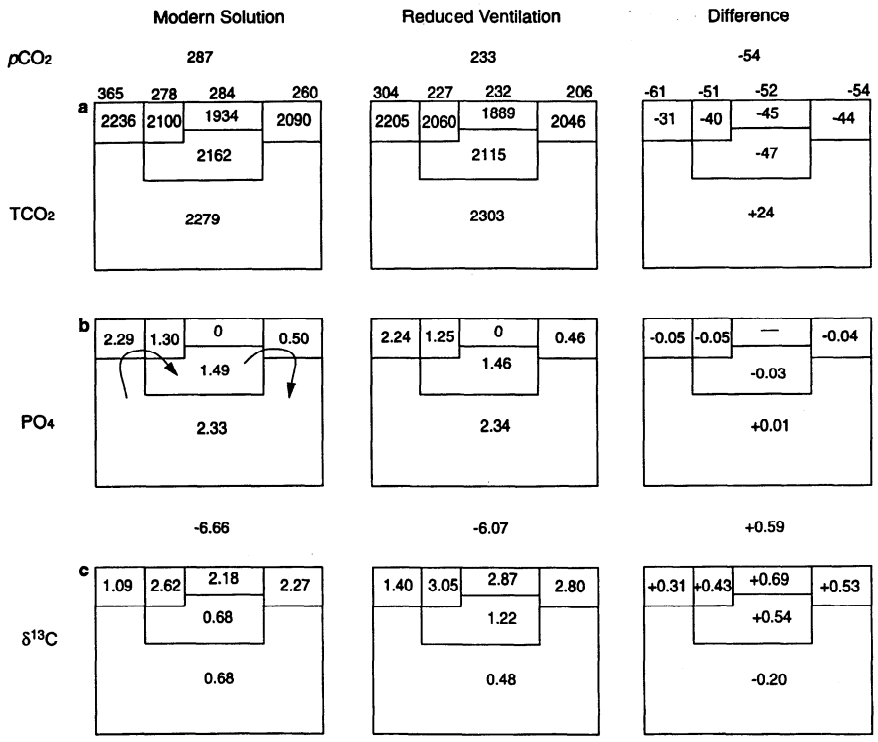

Figure 9. Solutions of the six-box model for (a) CO_2, (b) PO_4, and (c) $\delta^{13}C$ in a high-CO_2 state (in the left column, f_{pd} = 60 Sv and P_s = 3.0 moles C m^{-2} yr^{-1}) and a low-CO_2 state (middle column). The low-CO_2 state is produced by reducing f_{pd} to 12 Sv with P_s constant. T is fixed at 20 Sv, P_p is fixed at 1.0 moles C m^{-2} yr^{-1}, and P_n at 3.0 moles C m^{-2} yr^{-1}. Right column gives differences between the high- and low-CO_2 states. The alkalinity difference between the d box and the l box is 117 μeq kg^{-1} in both states.

$CaCO_3$ compensation response. *Boyle* [1988a] proposed that deeper remineralization of organic matter would shift nutrients and CO_2 from the upper ocean to the deep ocean and reduce the $CO_3^=$ content of deep water in contact with $CaCO_3$ sediments. Lower nutrient levels in the upper ocean reduce biological production in low latitudes and the flux of $CaCO_3$ to the seafloor. *Archer and Maier-Reimer* [1994] proposed that the $CO_3^=$ content of sediment pore waters was reduced by a general increase in the flux of organic matter reaching the seafloor. Enhanced dissolution in sediment pore waters reduces the accumulation of $CaCO_3$ at depths above the lysocline. In both *Boyle* [1988a] and *Archer and Maier-Reimer* [1994] a reduction in the $CaCO_3$ flux to the seafloor requires a deeper lysocline so that the area of seafloor accumulating $CaCO_3$ can expand to compensate for the reduction in burial. According to *Sigman* [1997] and *Sigman et al.* [1998] the $CaCO_3$ compensation mechanisms by *Boyle* [1988a] and *Archer and Maier-Reimer* [1994] would deepen the steady state glacial lysocline by hundreds of meters. The mean position of the glacial lysocline does not appear to have changed, however.

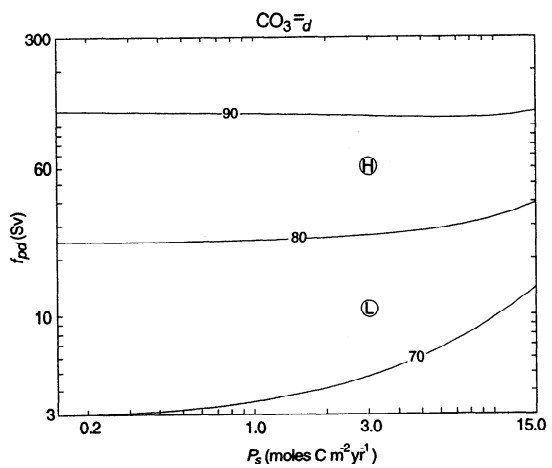

Figure 10. $CO_3^=$ concentration (in μmoles kg^{-1}) in the deep box of the six-box model as a function of f_{pd} versus P_s.

The $CaCO_3$ compensation mechanism in this paper does not involve systematic changes in the fluxes of organic carbon and $CaCO_3$ to the seafloor. Any steady state lysocline response to lower $CO_3^=$ in the deep ocean should be minimal. This means that the seven-box model can exploit $CaCO_3$ compensation without running afoul of the Sigman constraint.

4.4. $\delta^{13}C$ in the Seven-Box Model

Changes in $\delta^{13}C$ brought about by reduced ventilation of the deep box are given in Figure 13c. The $\delta^{13}C$ levels of the atmosphere and upper ocean rise by only 0.2‰, while the $\delta^{13}C$ of the deep box drops by 0.56‰ from +0.53 to –0.04‰. As with TCO_2, changes in $\delta^{13}C$ are largest in the small deep box. The model's chemical divide is expressed very clearly in

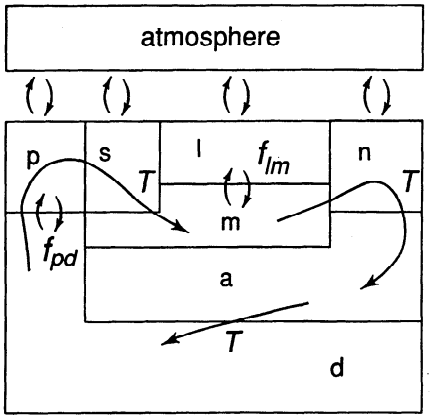

Figure 11. Schematic diagram of the seven-box model. Particle fluxes have been omitted for clarity.

the difference between the $\delta^{13}C$ change in the a box, +0.17‰, and the $\delta^{13}C$ change in the deep box, -0.56‰.

Broecker and Henderson [1998] outline a sequence of ancillary effects that operate on oceanic and atmospheric $\delta^{13}C$ during glacial time. The Broecker and Henderson sequence has been applied to the seven-box model in Table 5. The first column of Table 5 repeats the modern solution given in Figure 13c. Column two shows the effect of reducing f_{pd} from 60 to 10 Sv. Column three gives the effect of reduced surface temperatures, –4°C in the low-latitude and subantarctic boxes and –2°C in the North Atlantic and south polar boxes. Column four shows the effect of $CaCO_3$ compensation. Column five shows the effect of a 2‰ reduction in the organic fractionation factor (because of lower CO_2 concentrations in surface water). The terrestrial biosphere effect is incorporated in column six by simply subtracting 0.35‰ from the $\delta^{13}C$ of each box. Column seven gives the full glacial–interglacial $\delta^{13}C$ difference.

The total reduction of atmospheric CO_2 in Table 5 is 79 ppm. The $\delta^{13}C$ of the atmosphere declines by a whopping 0.71‰. The $\delta^{13}C$ of the low-latitude surface box declines by 0.26‰. The reduction of atmospheric $\delta^{13}C$ in Table 5 is in good agreement with the –0.7‰ glacial–interglacial difference measured by *Marino et al.* [1992], but it is not compatible with the –0.3‰ difference measured in ice cores [*Leuenberger et al.*, 1992]. The chemical divide in the full glacial state is reflected in the large contrast between the $\delta^{13}C$ change in the a box, –0.24‰, and in the d box, –0.86‰.

Table 6 summarizes the glacial–interglacial $\delta^{13}C$ changes expected for the three new models in this paper. The same ancillary effects have been applied in each case. Columns one and two give $\delta^{13}C$ changes for the four- and six-box models. Columns three and four give results the seven-box model. The a box in the seven-box model in column three is only 1000 m thick such that the top of the deep box is at 2000 m. Column four repeats results from Table 5 where the a box is 2000 m thick and the top of the deep box is at 3000 m. Column five gives observed $\delta^{13}C$ changes where available. The deep box becomes progressively smaller from left to right across Table 6. The deep box is 96% of the ocean's volume in the four-box model, roughly 75% in the six-box model, 50% in the seven-box model with an a box 1000 m thick, and 25% with an a box 2000 m thick. The same reductions in f_{hd} and f_{pd} used in Figures 6, 9, and 13 are applied in Table 6. The overall reduction in atmospheric CO_2 is ~80 ppm in each case.

Results from the four-box model in column one illustrate the expected pattern for conventional biopump models with a chemical divide at the bottom of a thin surface layer. Predict-

Table 4. Additional Input Parameters for Seven-Box Model

	Parameter Name	Value	Source
		Fixed Parameters	
Depth of Atlantic box	AAZ	2000 m	---
Volume of Atlantic box	VA	0.663×10^{18} m^3	AREA(1–FP)AAZ
Volume of deep box	VD	0.314×10^{18} m^3	VT–VL–VN–VS–VP–VM–VA
Fraction P_l, P_s remineralized in a box	---	0.10	$(1-\gamma_m)0.5$
Fraction P_l, P_s remineralized in deep box	---	0.10	$(1-\gamma_m)0.5$
Fraction P_n remineralized in a box	γ_a	0.50	---
Fraction P_n remineralized in deep box	---	0.50	$(1-\gamma_a)$
		Variable Parameters	
Vertical exchange between polar box and deep box	f_{pd}	3 - 300 Sv	
Sinking flux from subantarctic box	P_s	0.15 - 15.0 moles C m^{-2} yr^{-1}	

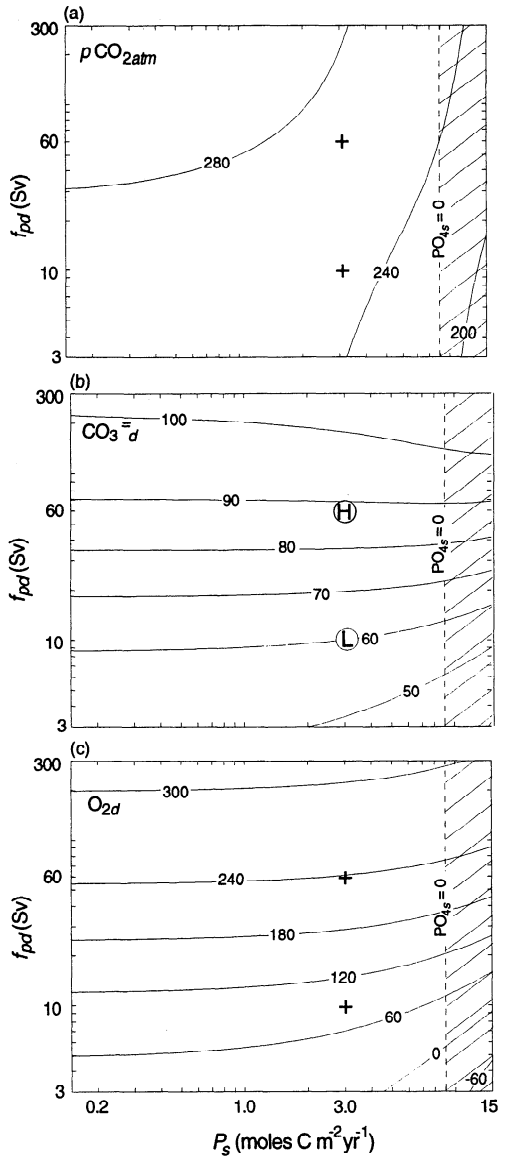

Figure 12. (a) Atmospheric CO_2, (b) $CO_3^{=}$, and (c) O_2 in the deep box of the seven-box model. Variables are contoured over a parameter space defined by variations in f_{pd} and P_s. P_p has been set to 1.0 moles C m^{-2} yr^{-1}, and P_n has been set to 3.0 moles C m^{-2} yr^{-1}. Additional input parameters are given in Tables 3 and 4.

ed $\delta^{13}C$ changes are positive in each surface box, up nearly 0.5‰ in low-latitude surface waters. The glacial atmosphere is heavier by 0.08‰. The ancillary effects of *Broecker and Henderson* [1998] almost manage to compensate for the +0.9-1.0‰ effect of a stronger biological pump, but they cannot make the glacial atmosphere lighter in $\delta^{13}C$.

The six-box model produces a glacial atmosphere 0.33‰ lighter than modern, a result in good agreement with the $\delta^{13}C$ change measured in ice cores [*Leuenberger et al.*, 1992]. The $\delta^{13}C$ change in the deep box of the six-box model, –0.54‰, is in good agreement with the average $\delta^{13}C$ change observed in deep water below 3000 m [*Boyle*, 1992]. The seven-box model with an a box 1000 m thick produces a glacial atmosphere –0.51‰ lighter than modern, a result midway between the *Leuenberger et al.* [1992] and *Marino et al.* [1992] estimates. The $\delta^{13}C$ change in low-latitude surface water is ~ –0.1‰, in the middle of the observed range. The $\delta^{13}C$ changes in the seven-box model with an a box 2000 m thick fall near the negative limit of the observed range.

The last two rows of Table 6 show predicted changes in pH for the deep boxes of all four models and for the a boxes of the two seven-box models. $CaCO_3$ compensation brings the deep pH of all four models up to or just below the interglacial pH. All boxes above become more alkaline. *Sanyal et al.* [1995] determined that the pH of the middepth water, 2600-3100 m in the Pacific and 3300-3800 m in the Atlantic, was 0.30 pH units higher than today. Sanyal et al.'s results suggest that the chemical divide in the glacial ocean was at least 3000 m deep, as in the seven-box model with the smallest deep box. Sanyal et al.'s results run counter to the six-box and seven-box solutions in columns two and three where positive pH changes are limited to water above 1000 and 2000 m, respectively.

As interpreted here, *Sanyal et al.'s* [1995] paleo pH results are consistent only with the model with the smallest deep box. Observed changes in $\delta^{13}C$ seem more consistent with the six- and seven-box models with a larger deep box. However, it is important to remember that the models in Table 6 reduce atmospheric CO_2 without any changes in biological production. Stronger biological activity and/or increased nutrient utilization in the Southern Ocean [e.g., *Kumar et al.*, 1995; *Francois et al.*, 1997] may have accounted for some of the glacial CO_2 drawdown. A small deep box allows the glacial atmosphere to remain depleted in $\delta^{13}C$ despite stronger biological production.

5. Discussion

Two key features separate the models in this paper from previous models. The first is the ability to decouple changes in atmospheric CO_2 from changes in polar nutrients. The second is the physical mechanism used to differentiate the carbon chemistry of middepth water from that of deep water. The discussion below describes these features in more detail and highlights some unrealistic features that arise in trying fit the two features above into a model with only seven boxes. It is hoped that the discussion sheds some light on how the mechanisms described in this paper might work in the real world.

5.1. Decoupling Atmospheric CO_2 From Polar Nutrients

The mechanism that decouples CO_2 from PO_4 is perhaps best understood by examining the covariance between TCO_2 and PO_4 concentrations in the seven-box model in Figure 14. Results from the high-CO_2 "modern" solution in Figure 13 are plotted as closed circles; results from the low-CO_2 "reduced ventilation" solution are plotted as open circles. Points from both solutions fall along two trends with slopes close to the Redfield slope used in the model, $r_{C:P}$ = 162.5. Points from the l, n, and a boxes fall along the "low-nutrient" trend. Points from the s and p boxes fall along the "high-nutrient" trend. Points from the m box plot between the two trends. The l and n boxes are low in nutrients because biological production strips PO_4 from the water entering these boxes. The a box is low in nutrients because it receives water directly from the n box. The s and p boxes are high in nutrients because they re-

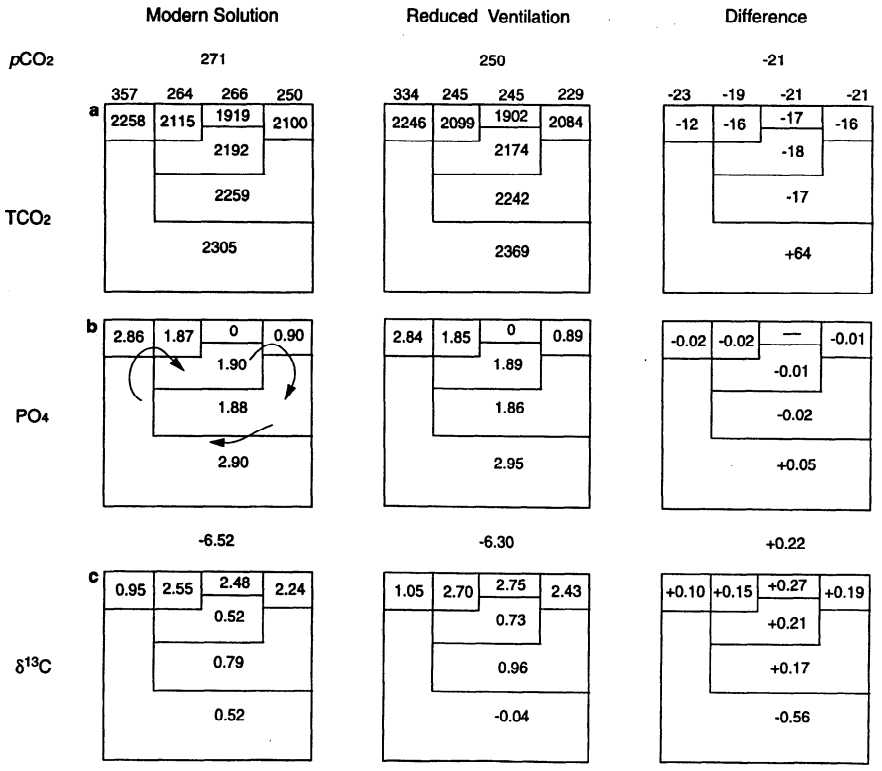

Figure 13. Solutions of the seven-box model for (a) CO_2, (b) PO_4, and (c) $\delta^{13}C$ in a high-CO_2 state (in the left column, f_{pd} = 60 Sv and P_s = 3.0 moles C m^{-2} yr^{-1}) and a low-CO_2 state (middle column, f_{pd} = 10 Sv and P_s unchanged). T is fixed at 20 Sv, P_p is fixed at 1.0 moles C m^2 yr^{-1}, and P_n at 3.0 moles C m^{-2} yr^{-1}. Right column gives differen-ces between the high- and low-CO_2 states. The alkalinity difference between the d box and the l box is 145 μeq kg^{-1} in the high-CO_2 state and 148 μeq kg^{-1} in the low-CO_2 state.

Table 5. Glacial $\delta^{13}C$ Changes According to the Seven-Box Model

Variable	Interglacial State[a]	Reduced Ventilation[b]	Reduced Surface Temperatures[c]	After $CaCO_3$ Compensation[d]	Reduced $\delta^{13}C$ Fractionation Factor[e]	Terrestrial Biosphere Effect[f]	Full Glacial Change[g]
$pCO2_{atm}$	270.6	249.7	226.9	191.4	191.4	----	−79.2
$\delta^{13}C_{atm}$	−6.52	−6.30	−6.68	−6.68	−6.88	−7.23	−0.71
$\delta^{13}C_l$	2.48	2.75	2.73	2.82	2.57	2.22	−0.26
$\delta^{13}C_n$	2.24	2.43	2.43	2.35	2.19	1.84	−0.40
$\delta^{13}C_s$	2.55	2.70	2.68	2.51	2.26	1.91	−0.64
$\delta^{13}C_p$	0.95	1.05	1.04	0.88	0.93	0.58	−0.37
$\delta^{13}C_m$	0.52	0.73	0.72	0.77	0.75	0.40	−0.12
$\delta^{13}C_a$	0.79	0.96	0.95	0.93	0.90	0.55	−0.24
$\delta^{13}C_d$	0.52	−0.04	−0.05	−0.08	0.01	−0.34	−0.86
pH_a	8.030	8.074	8.097	8.225	8.225	-----	+0.195
pH_d	8.062	7.875	7.899	8.047	8.047	-----	−0.015
$CO_3^{=}{}_d$	88.2	59.3	59.8	86.0	86.0	-----	−2.2

[a]High-CO_2 state in Figure 13; f_{pd} = 60 Sv.
[b]Low-CO_2 state in Figure 13; f_{pd} = 10 Sv.
[c]ΔTEMPL = −4°C, ΔTEMPS = −4°C, ΔTEMPN = −2°C, and ΔTEMPP = −2°C.
[d]Initial alkalinity in all ocean boxes increased by 120 μeq kg^{-1}. Initial TCO_2 in all ocean boxes increased by 60 μmoles kg^{-1}.
[e]Fractionation factor for ^{13}C during production of organic matter reduced 2‰ from -23 to -21‰.
[f]Here, 0.35‰ is subtracted from the $\delta^{13}C$ values in column five as a terrestrial biosphere effect.
[g]Difference between column six and column one.

Table 6. Glacial–Interglacial Changes in $\delta^{13}C$ Including Ancillary Effects

$\Delta Alk/\Delta TCO_2 \rightarrow$	Four-Box Model 12 / 6[a]	Six-Box Model 30 / 15[a]	Seven-Box Model AAZ=1000 m 70 / 35[a]	Seven-Box Model AAZ=2000 m 120 / 60[a]	Observed Change
$\Delta pCO2_{atm}$	−83.2	−84.2	−80.3	−79.2	−80
$\Delta\delta^{13}C_{atm}$	0.08	−0.33	−0.51	−0.71	−0.3[b] to −0.7[c]
$\Delta\delta^{13}C_l$	0.47	0.12	−0.07	−0.26	−0.4 to +0.2[d]
$\Delta\delta^{13}C_n$	0.39	−0.03	−0.21	−0.40	-----
$\Delta\delta^{13}C_s$	-----	−0.13	−0.31	−0.64	-----
$\Delta\delta^{13}C_p$	0.26	−0.09	−0.23	−0.37	-----
$\Delta\delta^{13}C_m$	-----	0.14	0.00	−0.12	-----
$\Delta\delta^{13}C_a$	-----	-----	−0.11	−0.24	-----
$\Delta\delta^{13}C_d$	−0.41	−0.54	−0.67	−0.86	−0.52[e]
ΔpH_a	-----	-----	+0.179	+0.195	+0.30 ± 0.1[f]
ΔpH_d	0.000	−.009	−0.006	−0.015	-----

[a]Amount of alkalinity and TCO_2 (in μeq kg^{-1} and μmoles kg^{-1}) added to each model in order to raise glacial $CO_3^{=}{}_d$ to within 3±1 μmoles kg^{-1} of the modern $CO_3^{=}{}_d$.

[b]*Leuenberger et al.* [1992].

[c]*Marino et al.* [1992].

[d]Range in glacial–interglacial $\delta^{13}C$ for planktonic foraminifera [*Broecker and Henderson*, 1998]. The glacial–interglacial difference could have been systematically more positive if higher glacial $CO_3^{=}$ reduced the $\delta^{13}C$ in foraminiferal calcite [*Spero et al.*, 1997].

[e]Observed $\delta^{13}C$ change for deep water below 3000 m [*Boyle*, 1992].

[f]*Sanyal et al.* [1995].

ceive upwelled water from the deep box, which accumulates remineralized nutrients from the low-nutrient boxes.

The key to the decoupling mechanism is the offset between the two trends and the composition of the deep box in relation to the two trends. The offset is due to the leveling effect of gas exchange, which raises the CO_2 content of the low-nutrient boxes and lowers the CO_2 content of the high-nutrient boxes. Thus TCO_2 concentrations along the two trends are similar despite a ~1 μmole kg^{-1} offset in PO_4. The TCO_2 and PO_4 content of the deep box, meanwhile, shifts up and down between the two trends. The deep box plots up close to the low-nutrient trend when there is weak ventilation through the polar box. This is what one expects given the advection of low-nutrient water into the deep box from the a box and the remineralization of sinking particles within the d box. With no outlet through the polar box, remineralized CO_2 remains bottled up within the deep box along with remineralized PO_4. With strong ventilation through the polar box the deep box composition plots lower, close to the high-nutrient trend. CO_2 remineralized in the deep box is able to escape to the atmosphere and upper ocean, while PO_4 remineralized in the deep box stays behind.

PO_4 remineralized in the deep box is compelled to stay in the deep box because there is no place for it go. Unlike CO_2, PO_4 concentrations in the l, n, and a boxes are constrained to be small and to stay more or less the same because PO_{4l} is always zero. Without wholesale changes in biological production or remineralization depth [*Boyle*, 1988a] the PO_4 content of the m box also stays more or less the same. PO_{4p}, meanwhile, is closely tied to PO_{4d} by strong upwelling and weak biological production in the polar box: if PO_{4d} is insensitive to changes in ventilation, so is PO_{4p}.

5.2. $\delta^{13}C$ and the Stratification of the Deep Ocean

Reconstructions of $\delta^{13}C$ for the glacial ocean show that deep water below 2500 m was lighter in $\delta^{13}C$ in relation to middepth and upper ocean water [*Curry et al.*, 1988; *Duplessey et al.*, 1988; *Kallel et al.*, 1988; *Oppo and Fairbanks*, 1990; *Herguera et al.*, 1992; *McCorkle et al.*, 1998; *Matsumoto and Lynch-Stieglitz*, 1999]. Middepth water in the glacial Atlantic seems to be squeezed upward by a thicker, more differentiated southern deep water [*Duplessey et al.*, 1988; *Bickert and Wefer*, 1996]. Cores in the South Atlantic and South Indian Oceans show that the deepest, densest water in the glacial ocean appears to have been the lightest water in the glacial ocean [*Charles et al.*, 1996; *Labeyrie et al.*, 1996]. Taken together, these observations suggest that the deep ocean during glacial time was both more stratified and more poorly ventilated.

Middepth water in the seven-box model is advected downward and is absorbed into the deep box without any mixing between the a and d boxes. This design is economical in terms of the number of boxes and parameters, but it has its limitations. In particular, it makes the south polar box the only pathway by which CO_2 remineralized in the deep ocean is allowed to return to the upper ocean; it also makes the south

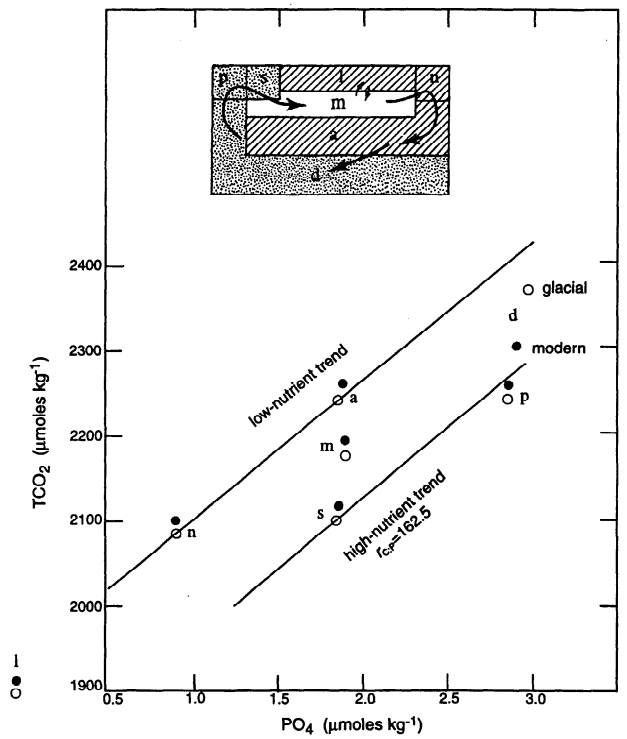

Figure 14. Relationship between TCO_2 and PO_4 among the seven boxes of the seven-box model. Results from the high-CO_2 modern solution in Figure 13 (f_{pd} = 60 Sv) are plotted as solid dots. Results from the low-CO_2 reduced ventilation solution (f_{pd} = 10 Sv) are plotted as open circles. Model points tend to fall along one of two trend lines with a slope of 162.5 (see text). Inset at top identifies boxes that are part of the low-nutrient (hatched area) and high-nutrient (stippled area) trends for the modern ocean.

polar box the sole conduit through which the low-$\delta^{13}C$ CO_2 in the deep ocean is allowed to mix with the relatively high-$\delta^{13}C$ CO_2 in the atmosphere and upper ocean. Figure 15 presents a more realistic view of how the upper/middepth ocean and the deep ocean interact. The circulation in Figure 15 has been redrawn so that the T circulation is confined to middepths and above. The circulation of deep water is depicted as a northward flow of bottom water and a southward return flow of deep water just above. In this way the volume of water upwelling around Antarctica is divided between two circulation regimes. The boundary separating middepth water from deep water is indicated by a pair of isopycnals. Mixing across the deep isopycnals is explicitly considered.

CO_2 remineralized in the deep regime of Figure 15 can get back to the surface two ways: it can mix across the deep isopycnals and upwell to the surface with the T circulation, or it can remain in the deep water and upwell to the surface as part of the bottom water circulation. Deep CO_2 upwelling with the T circulation flows away from Antarctica to the north and becomes part of the upper/middepth ocean. Deep CO_2 upwelling with the deep circulation vents to the atmosphere through the polar box as before. By providing a second pathway for remineralized CO_2 to reach the surface the exchange of water between the two circulation regimes shoulders some of the burden carried by the f_{hd} parameter in box models. A second pathway should significantly reduce the need for 60 Sv of f_{hd} in simulations of the modern ocean.

Figures 15b and 15c provide a more detailed view. Figure 15b depicts the Southern Ocean today, while Figure 15c presents a scenario for the glacial ocean. In Figure 15b the southward flow of northern middepth water and the southward return flow of southern deep water are shown in close proximity as if the two water masses are similar in density. Southern deep water is assumed to have ample opportunity to blend with the northern water so that CO_2 remineralized in deep water can become part of the upper ocean by the second pathway above. In Figure 15c, northern middepth water is depicted as being distinctly less dense than southern deep water. With a stronger physical separation between the two water masses the return of deep CO_2 to the surface should be limited to the polar pathway, and the mixing of low-$\delta^{13}C$ deep water with middepth water should be more restricted.

The scenario for the glacial ocean in Figure 15c brings to mind the glacial state described by *Oppo and Fairbanks* [1987, 1990] and *Broecker and Peng* [1989], who point to the low $\delta^{13}C$ levels observed in deep water of the glacial South Atlantic as evidence for a reduced input of NADW to the circumpolar region. They reason that a reduced input of NADW would make southern deep water more like middepth Pacific water with higher PO_4 and higher TCO_2. Broecker and Peng go on to argue that the glacial Southern Ocean had a larger surface to deep PO_4 gradient, stronger biological production, and a lower pCO_2 (the polar alkalinity hypothesis). *Oppo and Fairbanks* [1987,1990] and *Broecker and Peng* [1989] see the deep water upwelling to the surface in the south as a circumpolar water mass made up of more or less equal volumes of Atlantic outflow and Indo-Pacific outflow. When the North

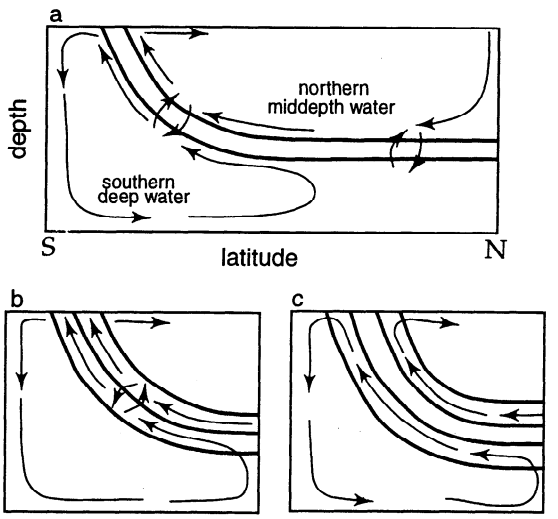

Figure 15. Set of diagrams illustrating how the blending of northern middepth water and southern deep water relates to the high-latitude mixing parameter f_{hd} (see text for details). (a) The blending of northern middepth water and southern deep water is depicted as simple mixing between adjacent southward flows. (b) A small density difference between northern middepth water and southern deep water aids the blending process in the modern ocean. (c) A larger north-south density difference inhibits the blending process in the glacial ocean.

Atlantic spigot is shut off, the circumpolar water mass becomes pure Indo-Pacific water. However, cores from the deep South Atlantic and South Indian Oceans show that low-$\delta^{13}C$ glacial Antarctic deep water had about the same Cd levels as the modern ocean [*Boyle*, 1992; *Rosenthal, et al.*, 1997]. This indicates that deep water in the Southern Ocean did not turn into a water type with the properties of middepth Pacific water.

Figure 15 views the Atlantic and Indo-Pacific outflows somewhat differently. The North Atlantic outflow is contained within the domain of northern middepth water. The Indo-Pacific outflow is contained within the domain of denser southern deep water. (Middepth Indo-Pacific water is something else again, see below.) An increase in the density contrast between north and south splits northern middepth water and Indo-Pacific deep water apart. It is suggested here that middepth water from the glacial North Atlantic continued to flow into the circumpolar region [*Yu et al.*, 1996], but unlike today, it was not dense enough to blend with the denser southern water. In this way an increase in the density contrast between middepth northern water and southern deep water, in combination with reduced ventilation through polar surface waters, would bottle up remineralized CO_2 in the ocean's deep water without much change in PO_4.

5.3. Middepth Water in the Indian and Pacific Oceans

The gateway to the middle depths of the ocean is depicted in the seven-box model as deep water formation in the North Atlantic. Water going into the middepth box remains more or less in equilibrium with atmospheric CO_2. When atmospheric CO_2 declines, TCO_2 levels in the middepth box decline along with TCO_2 in the upper ocean. From a CO_2 perspective the middepth box is part of the upper ocean. This is a reasonable expectation for middepth water in the Atlantic Ocean, but is it reasonable for middepth water in the Indian and Pacific Oceans?

At issue is the sign of TCO_2 and $\delta^{13}C$ changes in response to a change in ventilation in the Southern Ocean. If water at 2500 m in the Indo-Pacific was last in contact with the atmosphere in the subantarctic or subarctic North Pacific, its TCO_2 would decrease in response to reduced southern ventilation, just like NADW. If it was last in contact with the atmosphere in the Antarctic, its TCO_2 would increase in response to reduced southern ventilation. Oceanographic tradition dictates that middepth water in the Indian and Pacific is ventilated primarily from below and from the south [e.g., *Wyrtki*, 1962]. This may not be true.

A seminal paper by *Cox* [1989] shows how the boundary between deep water and middepth water the world over is set by the existence of Drake Passage and the ACC. Cox begins by considering an idealized world without Drake Passage. Southern deep water in Cox's no-Drake Passage world fills the entire deep ocean. When Drake Passage is opened, the domain of upper ocean water masses from north of Drake Passage expands downward at the expense of the denser southern water. When winds are added to drive a circumpolar current through Drake Passage, the domain of upper ocean water expands downward some more, leaving the domain of pure southern water as a relatively small volume near the bottom. Opening Drake Passage allows NADW, northern intermediate water, and subantarctic water to displace Antarctic water at middepths throughout the Atlantic, Indian, and Pacific.

Middepth water in the glacial Pacific was notably heavier in $\delta^{13}C$ than deep water in the Southern Ocean [*Duplessy et al.*, 1988]. It had a significantly higher $CO_3^=$ content than today. *Curry et al.* [1988] and *Duplessy et al.* [1988] concluded that these properties require a source of deep water or an expanded intermediate water in the North Pacific during glacial time. *Michel et al.* [1995] argues for a subantarctic source of deep water. However, these interpretations assume that middepth water in the modern Pacific is last in contact with the atmosphere in the far south. From this perspective a relatively heavy $\delta^{13}C$ requires a switch in ventilation. If middepth Pacific water last sees the atmosphere in the subantarctic and subpolar regions, then no switch in ventilation is needed. As shown in the seven-box model, reduced ventilation of southern deep water increases the $\delta^{13}C$ contrast between the upper ocean and deep ocean, making all middepth water heavier in $\delta^{13}C$. $CaCO_3$ compensation also increases the $CO_3^=$ content of middepth water. Middepth Pacific water is automatically more alkaline and heavier in $\delta^{13}C$ without a source of North Pacific deep water.

6. Conclusions

The seven-box model in this paper accounts for important features of the paleo record that have eluded previous models. It is able to reduce atmospheric CO_2 without a reduction in polar nutrients. It is able to produce a large depletion in the $\delta^{13}C$ of glacial bottom water without a substantial change in the nutrient content of glacial bottom water. The model also explains how the glacial atmosphere can have 80 ppm less CO_2 and still be lighter in $\delta^{13}C$ than the preindustrial atmosphere.

As interpreted here, glacial CO_2 and $\delta^{13}C$ observations point to a physical process, or a set of related physical processes, that stratify the interior while reducing the ventilation of the ocean's deepest water. These processes bottle up remineralized CO_2 at depths below 3000 m and reduce the $CO_3^=$ in deep water in contact with most of the ocean's $CaCO_3$ sediments. Through their control of the burial of $CaCO_3$ these ventilation and stratification processes are able to drive atmospheric CO_2 up and down on timescales between several thousand and 10 thousand years. Models by *Boyle* [1988a] and *Broecker and Peng* [1989] drive atmospheric CO_2 variations in much the same way, but they require changes in biological activity and major shifts in the ocean's nutrient fields. The mechanism described here will work without any changes in biological activity and minimal changes in the distribution of nutrients. The physical processes parameterized by the polar ventilation parameter in the box model have yet to be fully identified.

Acknowledgments. This paper is dedicated to K.-L. Selig, professor emeritus of Columbia University, a good friend who revealed to me the delights and rewards of a life in scholarship. I would like to thank W. Broecker, R. Keir, and E. Michel for their careful reviews of the submitted manuscript. S. Carson, D. Sigman, N. Gruber, C. Sabine, and M. Gloor provided in-house reviews. I would like to acknowledge a fruitful exchange with B. Curry as the inspiration for Figure 14. C. Raphael and J. Varanyak helped prepare the figures. W. Marshall prepared the camera-ready copy and helped with the equations and tables.

References

Archer, D. E., and E. Maier-Reimer, Effect of deep-sea sedimentary calcite preservation on atmospheric CO_2, *Nature, 367*, 260-264, 1994.

Bickert, T., and G. Wefer, Late Quaternary deep water circulation in the South Atlantic: Reconstruction from carbonate dissolution and benthic stable isotopes, in *The South Atlantic: Present and Past Circulation*, edited by G. Wefer et al., pp. 599-620, Springer-Verlag, New York, 1996.

Boyle, E. A., The role of vertical chemical fractionation in controlling late Quaternary atmospheric carbon dioxide, *J. Geophys. Res., 93*, 15,701-15,714, 1988a.

Boyle, E. A., Cadmium: Chemical tracer of deepwater paleoceanography, *Paleoceanography, 3*, 471-489, 1988b.

Boyle, E. A., Cadmium and $\delta^{13}C$ paleochemical ocean distributions during the stage 2 glacial maximum, *Annu. Rev. Earth Planet. Sci., 20*, 245-287, 1992.

Broecker, W. S., Glacial to interglacial changes in ocean chemistry, *Prog. Oceanogr., 11*, 151-197, 1982.

Broecker, W. S., The great ocean conveyor, *Oceanography, 4*, 79-89, 1991.

Broecker, W. S., and G. M. Henderson, The sequence of events surrounding Termination II and their implications for the cause of glacial-interglacial CO_2 changes, *Paleoceanography, 13*, 352-364, 1998.

Broecker, W. S., and T.-H. Peng, *Tracers in the Sea*, Lamont-Doherty Earth Obs., Palisades, N.Y., 1982.

Broecker, W. S., and T.-H. Peng, The role of $CaCO_3$ compensation in the glacial to interglacial CO_2 change, *Global Biogeochem. Cycles, 1*, 15-29, 1987.

Broecker, W. S., and T.-H. Peng, The cause of the glacial to interglacial atmospheric CO_2 change: A polar alkalinity hypothesis, *Global Biogeochem. Cycles, 3*, 215-239, 1989.

Catubig, N. R., D. E. Archer, R. Francois, P. de Menocal, W. Howard, and E.-F. Yu, Global deep-sea burial rate of calcium carbonate during the Last Glacial Maximum, *Paleoceanography, 13*, 298-310, 1998.

Charles, C. D., J. Lynch-Stieglitz, U. S. Ninnemann, and R. G. Fairbanks, Climate connections between the hemispheres revealed by deep-sea sediment core/ice core correlations, *Earth Planet. Sci. Lett., 142*, 19-27, 1996.

Cox, M. D., An idealized model of the world ocean, 1, The global-scale water masses, *J. Phys. Oceanogr., 19*, 1730-1752, 1989.

Curry, W. B., J. C. Duplessy, L. D. Labeyrie, and N. J. Shackleton, Changes in the distribution of $\delta^{13}C$ of deep water TCO_2 between the last glaciation and the Holocene, *Paleoceanography, 3*, 317-342, 1988.

Deacon, G. E. R., The hydrology of the Southern Ocean, *Discovery Rep., 15*, 1-124, plates I-XLIV, 1937.

Duplessy, J. C., N. J. Shackleton, R. G. Fairbanks, L. Labeyrie, D. Oppo, and N. Kallel, Deepwater source variations during the last climatic cycle and their impact on the global deepwater circulation, *Paleoceanography, 3*, 343-360, 1988.

Dymond, J., and M. Lyle, Flux comparisons between sediments and sediment traps in the eastern tropical Pacific: Implications for atmospheric CO_2 variations during the Pleistocene, *Limnol. Oceanogr., 30*, 699-712, 1985.

Francois, R. F., M. A. Altabet, E.-F. Yu, D. M. Sigman, M. P. Bacon, M. Frank, G. Bohrmann, G. Bareille, and L. D. Labeyrie, Water column stratification in the Southern Ocean contributed to the lowering of glacial atmospheric CO_2, *Nature, 389*, 929-935, 1997.

Herguera, J. C., E. Jansen, and W. H. Berger, Evidence for a bathyal front at 2000-m depth in the glacial Pacific, based on a depth transect on Ontong Java Plateau, *Paleoceanography, 7*, 273-288, 1992.

Jouzel, J., et al., Extending the Vostok ice-core record of paleoclimate to the penultimate glacial period, *Nature, 364*, 407-412, 1993.

Kallel, N., L. D. Labeyrie, A. Juillet-Leclerc, and J.-C. Duplessy, A deep hydrological front between intermediate and deep-water masses in the glacial Indian Ocean, *Nature, 333*, 651-654, 1988.

Keigwin, L. D., and E. A. Boyle, Late Quaternary paleochemistry of high-latitude surface waters, *Palaeogeogr. Palaeoclimatol. Palaeoecol., 73*, 85-106, 1989.

Keir, R. S., On the late Pleistocene ocean geochemistry and circulation, *Paleoceanography, 3*, 413-445, 1988.

Keir, R. S., Reconstructing the ocean carbon system variation during the last 150,000 years according to the Antarctic nutrient hypothesis, *Paleoceanography, 5*, 253-276, 1990.

Knox, F., and M. B. McElroy, Changes in atmospheric CO_2: Influence of the marine biota at high latitude, *J. Geophys. Res., 89*, 4629-4637, 1984.

Kumar, N., R. F. Anderson, R. A. Mortlock, P. N. Froelich, P. Kubik, B. Dittrich-Hannen, and M. Suter, Increased biological productivity and export production in the glacial Southern Ocean, *Nature, 378*, 675-680, 1995.

Labeyrie, L., et al., Hydrographic changes of the Southern Ocean (southeast Indian sector) over the last 230 kyr, *Paleoceanography, 11*, 57-76, 1996.

Leuenberger, M., U. Siegenthaler, and C. C. Langway, Carbon isotope composition of atmospheric CO_2 during the last ice age from an Antarctic core, *Nature, 357*, 488-490, 1992.

Levitus, S., Climatological atlas of the world ocean, *NOAA Prof. Pap. 13*, U.S. Gov. Print. Off., Washington, D.C., 1982.

Levitus, S., J. L. Reid, M. E. Conkright, and R. Najjar, Distribution of nitrate, phosphate, and silicate in the world oceans, *Prog. Oceanogr., 31*, 245-273, 1993.

Lyle, M., and N. Pisias, Ocean circulation and atmospheric CO_2 changes: Coupled use of models and paleoceanographic data, *Paleoceanography, 5*, 15-41, 1990.

Marino, B. D., M. B. McElroy, R. J. Salawitch, and W. G. Spaulding, Glacial-to-interglacial variations in the carbon isotopic composition of atmospheric CO_2, *Nature, 357*, 461-466, 1992.

Martin, J. H., Glacial-interglacial CO_2 change: The iron hypothesis, *Paleoceanography, 5*, 1-13, 1990.

Matsumoto, K., and J. Lynch-Stieglitz, Similar glacial and Holocene deep water circulation inferred from southeast Pacific benthic foraminiferal carbon isotope composition, *Paleoceanography, 14*, 149-163, 1999.

McCorkle, D. C., D. T. Heggie, and H. H. Veeh, Glacial and Holocene stable isotope distributions in the southeastern Indian Ocean, *Paleoceanography, 13*, 20-34, 1998.

Michel, E., L. D. Labeyrie, J.-C. Duplessy, N. Gorfti, M. Labracherie, and J.-L. Turon, Could deep subantarctic convection feed the world deep basins during the Last Glacial Maximum?, *Paleoceanography, 10*, 927-942, 1995.

Oppo, D. W., and R. G. Fairbanks, Variability in the deep and intermediate water circulation of the Atlantic Ocean during the past 25,000 years: Northern Hemisphere modulation of the Southern Ocean, *Earth Planet. Sci. Lett., 86*, 1-15, 1987.

Oppo, D. W., and R. G. Fairbanks, Atlantic Ocean thermohaline circulation of the last 150,000 years: Relationship to climate and atmospheric CO_2, *Paleoceanography, 5*, 277-288, 1990.

Paillard, D., M. Ghil, and H. Le Treut, Dissolved organic matter and the glacial-interglacial pCO_2 problem, *Global Biogeochem. Cycles, 7*, 901-914, 1993.

Rosenthal, Y., E. A. Boyle, and L. Labeyrie, Last Glacial Maximum paleochemistry and deep-water circulation in the Southern Ocean, *Paleoceanography, 12*, 787-796, 1997.

Sanyal, A., N. G. Hemming, G. N. Hanson, and W. S. Broecker, Evidence for a higher pH in the glacial ocean from boron isotopes in foraminifera, *Nature, 373*, 234-236, 1995.

Sarmiento, J. L., and J. C. Orr, Three-dimensional simulations of the impact of Southern Ocean nutrient depletion on atmospheric CO_2 and ocean chemistry, *Limnol. Oceanogr., 36*, 1928-1950, 1991.

Sarmiento, J. L., and J. R. Toggweiler, A new model for the role of the oceans in determining atmospheric pCO_2, *Nature, 308*, 621-624, 1984.

Shackleton, N. J., Carbon-13 in Uvigerina: Tropical rainforest history and the equatorial Pacific carbonate dissolution cycle, in *The Fate of Fossil Fuel CO_2 in the Oceans*, edited by N. R. Anderson and A. Malahoff, pp. 401-428, Plenum, New York, 1977.

Siegenthaler, U., and T. Wenk, Rapid atmospheric CO_2 variations and ocean circulation, *Nature, 308*, 624-626, 1984.

Sigman, D. M., The role of biological production in Pleistocene atmospheric carbon dioxide variations and the nitrogen isotope dynamics of the Southern Ocean, Ph.D. dissertation, 385 pp., Woods Hole Oceanogr. Inst./Mass. Inst. of Technol. Joint Program, Woods Hole, 1997.

Sigman, D. M., D. C. McCorkle, and W. R. Martin, The calcite lysocline as a constraint on glacial/interglacial low-latitude production changes, *Glob. Biogeochem. Cycles, 12*, 409-427, 1998.

Spero, H. J., J. Bijma, D. W. Lea, and B. E. Bemis, Effect of seawater carbonate concentration on foraminiferal carbon and oxygen isotopes, *Nature, 390*, 497-500, 1997.

Sverdrup, H. U., M. W. Johnson, and R. H. Fleming, *The Oceans: Their Physics, Chemistry and General Biology*, 1087 pp., Prentice-Hall, Englewood Cliffs, N.J., 1942.

Takahashi, T., W. S. Broecker, A. E. Bainbridge, and R. F. Weiss, Carbonate chemistry of the Atlantic, Pacific, and Indian Oceans: Results of the GEOSECS expeditions, 1972-1978, *Tech. Rep. 1 CU-1-80*, Lamont-Doherty Geol. Obs., Palisades, N.Y., 1980.

Takahashi, T., W. S. Broecker, and S. Langer, Redfield ratio based on chemical data from isopycnal surfaces, *J. Geophys. Res., 90*, 6907-6924, 1985.

Toggweiler, J. R., and B. Samuels, New radiocarbon constraints on the upwelling of abyssal water to the ocean's surface, in *The Global Carbon Cycle, NATO ASI Ser.*, vol. I15, edited by M. Heimann, pp. 333-366, Springer-Verlag, New York, 1993.

Toggweiler, J. R., and B. Samuels, Effect of Drake Passage on the global thermohaline circulation, *Deep Sea Res., Part I, 42*, 477-500, 1995.

Toggweiler, J. R., and J. L. Sarmiento, Glacial to interglacial changes in atmospheric carbon dioxide: The critical role of ocean surface water in high latitudes, in *The Carbon Cycle and Atmospheric CO_2: Natural Variations Archean to Present, Geophys. Monogr. Ser.*, vol. 55, edited by E. T. Sundquist and W. S. Broecker, pp. 163-184, AGU, Washington, D.C., 1985.

Weast, R. C., and M. J. Astle (eds.), *CRC Handbook of Chemistry and Physics*, 60th ed., CRC Press, Boca Raton, Fla., 1979.

Wyrtki, K., The thermohaline circulation in relation to the general circulation of the oceans, *Deep Sea Res., 8*, 39-64, 1961.

Wyrtki, K., The oxygen minimum in relation to the ocean circulation, *Deep Sea Res., 9*, 11-23, 1962.

Yu, E.-F., R. Francois, and M. P. Bacon, Similar rates of modern and last-glacial ocean thermohaline circulation inferred from radiochemical data, *Nature, 379*, 689-694, 1996.

J. R. Toggweiler, Geophysical Fluid Dynamics Laboratory, National Oceanic and Atmospheric Administration, P. O. Box 308, Princeton, NJ 08542. (jrt@gfdl.gov)

(Received February 17, 1999;
revised June 1, 1999;
accepted June 4, 1999.)